UNIVERSIDADE DE LISBOA
FACULDADE DE CIÊNCIAS
DEPARTAMENTO DE BIOLOGIA VEGETAL

Unravelling the role of Ctdnep1-Eps8L2 interaction during nuclear positioning in migrating fibroblasts

Ana Sofia Carvalho Marques

Mestrado em Biologia Molecular e Genética

Dissertação orientada por:
Doutor Edgar R. Gomes
Professora Maria Helena Trindade

2019

Unravelling the role of Ctdnep1-Eps8L2 interaction during nuclear positioning in migrating fibroblasts

Ana Sofia Carvalho Marques

Acknowledgements

Thank you, Edgar Gomes, my external supervisor, for giving me the opportunity of being a part of your amazing team at Instituto de Medicina Molecular João Lobo Antunes. For all the scientific discussions and guidance, which played an important role in improving my work. Thank you for all the advices about my scientific career and for always encourage me to think about my future with no restrictions.

Thank you, Francisco Calero, my co-supervisor, for the nonstop guidance in the past year. You were an amazing teacher, sharing your knowledge and experience with me. You provided the best learning environment, listening to all my questions, giving me space to increase my independence and encouragement when the experiments did not work that well or when I kept saying that I did not have any results. Thank you for all the patience, time, knowledge and laughter in this past year.

Thank you to Professor Maria Helena Trindade, my internal supervisor, for all your kindness and support. For always having time to listen to me and help me throughout this year.

Thank you to everyone in Edgar Gomes lab (Cátia Janota, Helena Pinheiro, Mafalda Pimentel, Judite Costa, Sara Ferreira and more) and Cláudio Franco lab (Catarina Fonseca, Pedro Barbacena, Marta Fidalgo, Francisca Vasconcelos and more) for making me feel welcome since my first day in the lab and for always being supportive and ready to help. You have helped me in the simplest ways, from scientific discussions to sharing food and funny moments. Lou Wackerbarth, how could I forget you? You were the best "partner in crime". When I was dying inside at every second, even at such a long distance, you were always there! Thank you for all the conversations, Minicampus nights, adventures and all the laughs.

Thank you to all the scientific (Joana Saraiva, Isa Moutinho, Margarida Machado, Inês Peixoto, Nina Karguth and many more) and non-scientific (Marta Viana, Tânia Costa) friends that kindly supported me throughout this year. Special thanks to Francisco Ferreira, Bianca Gama and Beatriz Duarte for being a "safe place" to send all those desperate late-night long texts, helping me to "despanicar" and not go completely insane. Thank you for understanding me in the most ridiculous things and laughing with me at all circumstances.

Thank you to my family for caring, even without understanding a great deal of what I did in this thesis. An enormous thank you to my parents, for believing in me and encouraging me to follow my dreams, always pushing me to go further. I do not know how you could cope with me in a daily basis this past year. You listened to me in my lowest moments and celebrated even my tiniest victories. Thank you for saying stop when I just could not see the limits anymore and pushed myself too far. Thank you also to my Aunt Alzira and Uncle José for being my second parents and unconditionally believing in me.

All of you made an enormous difference this past year, so this thesis is also yours! Let us celebrate it!

Abstract

Positioning the nucleus within the cell is crucial for cell division, differentiation and proper migration. Different cells initiate their motility by positioning the nucleus to the cell rear, setting up a leading edge-centrosome-nucleus polarization in the direction of migration. This nuclear movement is promoted by retrograde moving dorsal actin cables that bind to the Linker of Nucleoskeleton and Cytoskeleton (LINC) complex at the nuclear envelope, forming what is known as Transmembrane Actin-associated Nuclear (TAN) lines. In the last years, several proteins have been identified as regulators of the LINC complex for TAN lines formation. However, little is known about how actin is organized or if there is any other LINC complex-independent mechanism in this process.

Recently in Gomes lab, two proteins were identified as novel players in nuclear movement: the C-Terminal Domain Nuclear Envelope Phosphatase 1 (Ctdnep1) and the Epidermal Growth Factor Receptor Kinase Substrate 8-Like Protein 2 (Eps8L2). These proteins were shown to physically and directly interact, being determinant for TAN line-dependent nuclear positioning in migrating fibroblasts by regulating dorsal actin cables organization. However, is not yet well understood how Ctdnep1-Eps8L2 interaction is coupled to nuclear positioning. Here, we further characterize this interaction regarding its subcellular localization, mechanistic basis and role in cell migration. Through the Clustered Regularly Interspaced Short Palindromic Repeats (CRISPR)/CRISPR Associated Protein 9 (Cas9) system, it is attempted to tag the endogenous Ctdnep1 and Eps8L2 in NIH 3T3 cells to study its subcellular localization. However, this approach was unsuccessful, since no positively tagged cells were observed after Fluorescence-Activated Cell Sorting (FACS) selection. As an alternative, using NIH 3T3 stable cell lines expressing tagged versions of Ctdnep1 or Eps8L2, it is demonstrated that Ctdnep1 localizes to the nuclear envelope and endoplasmic reticulum (regardless of its phosphatase activity), while Eps8L2 localizes to the cytoplasm. Given that Ctdnep1 localization is restricted to the nuclear envelope and endoplasmic reticulum, especially near the nucleus, it is suggested that this should be the region where Ctdnep1 and Eps8L2 interact. Taking advantage of the CRISPR/Cas9 tools developed, currently, Eps8L2 and Ctdnep1 knockout cell lines are being generated to further inquire if the subcellular localization of the two proteins influences one another. Furthermore, it is hypothesized that Ctdnep1 may control Eps8L2 activity by dephosphorylation, regulating perinuclear actin organization and, thus, affecting nuclear positioning and cell migration. Through mass spectrometry analysis, S479 and S480 are identified as possible phosphorylation sites for Eps8L2 and, thus, potential substrates for Ctdnep1 phosphatase activity. Additionally, wound-healing assays were performed to further enquire about Ctdnep1 and Eps8L2 role in cell migration. In the present experimental conditions, Ctdnep1-Eps8L2 interaction did not present a role in 2D-cell migration.

Collectively, this work provides data that further pursues the role of Ctdnep1 and Eps8L2 interaction in actin organization as well as its implications during nuclear positioning. Other details regarding this interaction should also be explored, such as its possible function in mechanotransduction and gene expression, its coordination with other previously reported mechanisms for regulating LINC complex and TAN lines dynamics or its role in 3D cell migration. Ultimately, this work sheds light on the importance of identifying new players in the complex and refined network that regulates nuclear positioning. Deciphering the mechanisms connecting the nucleus to the cytoskeleton is valuable to better understand important physiological correlations between nuclear positioning and disease.

Keywords: nuclear positioning, TAN lines, LINC complex, Ctdnep1, Eps8L2.

Resumo

As células eucarióticas posicionam ativamente e de forma precisa o seu núcleo no citoplasma. Este posicionamento é crucial para processos como a divisão, diferenciação e migração celulares. Durante a migração celular, o núcleo torna-se particularmente importante ao estar envolvido no estabelecimento de polaridade, integração de forças intracelulares e deformação nuclear para permitir o movimento da célula por constrições reduzidas. Estes processos dependem largamente do tipo de célula e do substrato de migração. Diferentes células iniciam a sua motilidade com o posicionamento do núcleo na zona posterior da célula, enquanto o centrossoma (estático) assume uma localização entre a frente migrante e o núcleo (onde o centrossoma se diz reorientado). Logo, surge na célula uma polarização frente migrante-centrossoma-núcleo na direção de migração. Este movimento nuclear é promovido por cabos dorsais de actina em movimento retrógrado que se ligam a proteínas do invólucro nuclear provenientes do complexo de Ligação do Nucleoesqueleto e Citoesqueleto (LINC), formando linhas Nucleares Transmembranares associadas a Actina (TAN). Apesar do complexo LINC ser o protagonista no modelo atual de acoplamento entre o núcleo e o citoesqueleto, outras proteínas têm sido identificadas na regulação do complexo LINC para a formação das linhas TAN. Contudo, o conhecimento sobre como a actina é organizada ou se existe outro mecanismo independente do complexo LINC é escasso.

Recentemente no laboratório Gomes, foram identificadas duas novas proteínas envolvidas no movimento nuclear. São elas a Fosfatase 1 do Invólucro Nuclear de Domínio C-terminal (Ctdnep1) e a Proteína 2 de Substrato Tipo 8 de Recetor Cinase do Fator de Crescimento Epidérmico (Eps8L2). A Ctdnep1 (previamente designada por Dullard) é uma fosfatase localizada no invólucro nuclear e no retículo endoplasmático. Esta proteína foi descrita pela primeira vez em *Xenopus laevis* por participar no desenvolvimento do tubo neuronal. Atualmente, a Ctdnep1 é mais conhecida pelo seu papel na desfosforilação e ativação das Lipinas-1 e -2 em mamíferos e, consequentemente, na regulação do metabolismo global de ácidos gordos. Para esta desfosforilação ocorrer, é requerida a presença da Subunidade Reguladora da Fosfatase 1 do Invólucro Nuclear (Nep1-r1). A Eps8L2 é uma proteína do citoesqueleto pertencente à família de proteínas Eps8. Funcionalmente, a Eps8L2 é mais conhecida pelo seu papel no complexo Sos1-Abi1-PI3K-Eps8L2, necessário para a ativação da GTPase Rac, resultando na remodelação da actina no citoesqueleto. Adicionalmente, para regular a dinâmica da actina, a Eps8L2 é capaz de limitar a polarização dos filamentos de actina através do bloqueio dos terminais de rápido crescimento (atividade conhecida como *capping* da actina) e promover ligações cruzadas entre filamentos de actina formando estruturas mecanicamente mais resistentes (atividade conhecida como *bundling* da actina). A atividade de *bundling* da actina encontra-se amplamente descrita na manutenção dos estereocílios na cóclea.

Previamente no laboratório Gomes, demonstrou-se que, em fibroblastos migrantes, o *knockdown* de Ctdnep1 ou Eps8L2 resulta numa deficiência no movimento retrógrado do núcleo e na reorientação do centrossoma, fenómenos relacionados com uma possível regulação da organização dos cabos dorsais de actina por Ctdnep1 e Eps8L2. Assim, na ausência destas proteínas, o principal mecanismo de posicionamento nuclear e migração celular em fibroblastos encontra-se danificado. Adicionalmente, foi identificada uma interação física e direta entre Ctdnep1 e Eps8L2. Contudo, não tinha sido totalmente explorado o modo como esta interação está relacionada com o posicionamento nuclear.

Neste trabalho, caracteriza-se a interação entre Ctdnep1 e Eps8L2 relativamente à sua localização subcelular, mecanismo e papel durante a migração celular. Para estudar a localização subcelular da Ctdnep1 e da Eps8L2 em fibroblastos migrantes, realizou-se o *knockin* de marcadores (GFP e miRFP670, respetivamente) nas proteínas endógenas em células NIH 3T3, utilizando o sistema de Repetições Palindrómicas Curtas Agrupadas e Regularmente Interespaçadas (CRISPR)/Proteína 9

Associada a CRISPR (Cas9). Para enriquecer a população celular em células positivas para GFP ou miRFP670, realizou-se Separação Celular Ativada por Fluorescência (FACS). Contudo, apesar de serem recolhidas entre 1000 e 2000 células positivas por *knockin*, não foi possível observar células positivas ao microscópio, sendo frequentemente observada uma morte celular extensa após um curto período em cultura. Adicionalmente, uma segunda seleção por FACS não enriqueceu o número de células positivas. Para testar se a Cas9 não estava a realizar o corte em dupla cadeia na sequência-alvo e, consequentemente, as células não apresentavam a edição desejada, células NIH 3T3 foram transduzidas com as sequências codificantes para a Cas9 e os gRNAs utilizados anteriormente. Por sequenciação do DNA genómico, observou-se que a Cas9 estava efetivamente a cortar as sequências genómicas na região pretendida, validando os gRNAs utilizados. Adicionalmente, para investigar se as localizações subcelulares da Ctdnep1 e da Eps8L2 são influenciadas entre si, estão a ser geradas linhas celulares com *knockouts* para *EPS8L2* ou *CTDNEP1* em células transduzidas com gRNAs que têm como alvo a região do codão de iniciação.

Numa segunda abordagem ao estudo da localização subcelular, geraram-se linhas celulares NIH 3T3 a expressar estavelmente sequências codificantes para Ctdnep1-GFP, Ctdnep1_D67E-GFP (a variante mutada sem atividade de fosfatase) ou Eps8L2-GFP. Utilizando estas linhas celulares, demonstrou-se que a Ctdnep1 se localiza no invólucro nuclear e no retículo endoplasmático, independentemente da sua atividade de fosfatase. Já a Eps8L2 apresenta uma localização distribuída pelo citoplasma. Assim, tendo em conta a restrição da localização da Ctdnep1 ao invólucro nuclear e ao retículo endoplasmático, especialmente perto do núcleo, sugere-se que esta seja a região de interação entre a Ctdnep1 e a Eps8L2. Contudo, algumas células não apresentavam os mesmos padrões de expressão, sendo esta visivelmente mais baixa, traduzindo a perda da expressão das proteínas marcadas ao longo do tempo. Consequentemente, as linhas celulares não se encontravam totalmente estáveis, sendo necessária uma seleção mais restrita de células positivas para GFP.

Adicionalmente, questionou-se sobre a natureza da interação direta entre Ctdnep1 e Eps8L2. Tendo em consideração a atividade de fosfatase da Ctdnep1, colocou-se a hipótese de que a Ctdnep1 desfosforila a Eps8L2, o que resulta na ativação da capacidade da Eps8L2 para promover o *bundling* da actina. Consequentemente, formam-se cabos de actina espessos o suficiente para uma ligação eficiente ao complexo LINC, promovendo o movimento do núcleo. Para testar esta hipótese, Eps8L2 e Ctdnep1 (*wild type* ou D67E) exclusivamente ou na presença da subunidade reguladora Nep1-r1 foram co-expressas em células U2OS. Por espetrometria de massa, foi possível identificar os fosforesíduos em Eps8L2 e estudar diferenças no estado de fosforilação entre condições. Mais especificamente, os fosforesíduos S479 e S480 apresentaram um sinal de fosforilação significantemente inferior na presença de Ctdnep1 e Nep1-r1, comparativamente a Ctdnep1_D67E. Assim, estas serinas apresentam-se como possíveis substratos para a desfosforilação da Eps8L2 pela Ctdnep1.

Quanto ao seu papel na migração celular, através de ensaios de cicatrização de feridas, demonstrou-se que aquando do *knockdown* de Ctdnep1 ou Eps8L2, não existe um impacto na migração celular em 2D. Contudo, esta observação não descarta a hipótese de Ctdnep1 e Eps8L2 desempenharem papéis determinantes para a migração celular em 3D. De facto, em substratos 3D as propriedades da matriz extracelular podem impor constrições únicas na migração celular, com a consequente utilização de vias moleculares fundamentalmente diferentes da migração em 2D, para deformar ou posicionar o núcleo. Assim, a possibilidade da interação Ctdnep1-Eps8L2 ser determinante para a migração em matrizes 3D deverá ser explorada.

Coletivamente, neste trabalho aprofunda-se o papel da interação entre Ctdnep1 e Eps8L2 na organização da actina, bem como, as suas implicações durante o posicionamento nuclear. Outros pormenores necessitam de ser explorados, tais como, a possível função desta interação na mecano-transdução e

expressão génica, a coordenação entre a interação Ctdnep1-Eps8L2 e outras previamente descritas para a regulação da dinâmica do complexo LINC e linhas TAN ou o papel da interação na migração em matrizes 3D. Em última instância, este estudo reforça a necessidade de identificar novos intervenientes na complexa e refinada rede molecular que regula o posicionamento nuclear. A identificação e caracterização destes intervenientes é crucial para uma melhor compreensão de correlações fisiológicas importantes, particularmente entre posicionamento nuclear e doença.

Palavras-chave: posicionamento nuclear, linhas TAN, complexo LINC, Ctdnep1, Eps8L2.

Table of contents

List of tables

List of figures

List of abbreviations

2D: two-dimensional

3D: three-dimensional

A (amino acid): alanine

A (DNA base): adenine

Abi1: Abelson interactor 1

AID: auxin-inducible degron

ANC-1: nuclear anchorage protein 1

ATP: adenosine triphosphate

BMP: bone morphogenic protein

bp: base pair

C: cytosine

Cdc42: cell division control protein 42 homolog

cDNA: complementary DNA

CRISPR/Cas9: clustered regularly interspaced short palindromic repeats/CRISPR associated protein 9

Ctdnep1: C-terminal domain nuclear envelope phosphatase 1

CtIP: CtBP-interacting protein

D: aspartic acid

DAPI: 4',6'-diamino-2-fenil-indol

DMEM: Dulbecco's modified eagle medium

DNA: deoxyribonucleic acid

***DNM2*:** dynamin 2

DSB: double-strand break

E: glutamic acid

ECL: enhanced chemiluminescent

ECM: extracellular matrix

EGFR: epidermal growth factor

Eps8L2: epidermal growth factor receptor kinase substrate 8-like protein 2

ER: endoplasmic reticulum

ESCRT-III: endosomal sorting complex required for transport-III

FACS: fluorescence-activated cell sorting

F-actin: filamentous actin

FCP1: transcription factor IIF-associating CTD phosphatase 1

FHOD1: FH1/FH2 domain-containing protein 1

FW: forward

G: guanine

G1: gap 1

G2: gap 2

G-actin: globular actin

GEF: nucleotide exchange factor

GFP: green fluorescent protein

gRNA: guide RNA

GTPase: guanosine triphosphate hydrolase

HDR: homology-directed repair

HEK 293: human embryonic kidney 293 cells

HRP: horseradish peroxidase

IF: immunofluorescence

INDEL: insertion or deletion

INM: inner nuclear membrane

KASH: Klarsicht/ANC-1/Syne homology

LAP1: lamina associated polypeptide 1

LINC: linker of nucleoskeleton and cytoskeleton

***LMNA*:** lamin A/C

LPA: lysophosphatidic acid

miRFP: monomeric near-infrared fluorescent protein

***MTM1*:** myotubularin 1

MW: molecular weight

n: number of cells

NCBI: national center for biotechnology information

NE: nuclear envelope

Nep1-r1: nuclear envelope phosphatase 1-regulatory subunit 1

Nesprin-2G: nesprin-2 giant

NHEJ: non-homologous end joining

NIH 3T3: mouse fibroblasts

NLS: nuclear localization signal

ns: not statistically significant

ONM: outer nuclear membrane

P: p-value

PAM: protospacer adjacent motif

PBS: phosphatase buffer saline

PCR: polymerase chain reaction

PDMS: polydimethylsiloxane

PI3K: phosphatidylinositol-4,5-bisphosphate 3-kinase

PNS: perinuclear space

PTB: phosphotyrosine binding

qPCR: quantitative PCR

RNA: ribonucleic acid

rpm: revolutions per minute

RT: room temperature

RW: reverse

S (amino acid): serine

S (cell cycle): synthesis

Samp1: spindle-associated membrane protein 1

SDS: sodium dodecyl sulfate

SEM: standard error of the mean

SH3: Src homology 3

siRNA: small interference RNA

Sos1: son of sevenless homolog 1

SUN: Sad1/UNC-84

T (amino acid): threonine

T (DNA base): thymine

Ta: temperature of annealing

TAN: transmembrane actin-associated nuclear

TBE: tris-borate-EDTA

TBS: tris-buffered saline

TBST: TBS with 0,1% Tween® 20

Tm: temperature of melting

TM: transmembrane

U2OS: human bone osteosarcoma epithelial cells

V: valine

VSV-G: vesicular stomatitis virus glycoprotein

WB: western blotting

WNT: wingless-related integration site

WT: wild type

1. Introduction

1.1. The nucleus and its architecture

The nucleus is the main distinguishing feature of eukaryotic cells, being both the largest and the stiffest organelle in animal cells. It is responsible for housing genetic information, maintaining its integrity and facilitating its transcription and replication[1].

Structurally, the nucleus is bordered by a double bilayer, the Nuclear Envelope (NE), that encloses the nucleoplasm. The nucleoplasm comprises chromatin, the nucleoskeleton and other substructures such as the nucleolus. The NE consists of a cytoplasm-facing Outer Nuclear Membrane (ONM) and a nucleoplasm-facing Inner Nuclear Membrane (INM), separated by a gap of 30-50 nm called perinuclear space (PNS) (Figure 1.1)[1,2]. In animal cells, the NE features an additional component, the nuclear lamina. This is a thin meshwork of intermediate filament proteins (A-type and B-type lamins) that associate with the nuclear face of the INM and provide structural integrity to the NE, thus contributing to the global nuclear architecture[3]. Lamins have additional functions by regulating chromatin and being involved in various signaling pathways that culminate in gene expression effects[4].

The existence of a cell nucleus allows for chromatin control through a refined regulation, although this compartmentalization poses logistical challenges made by the need to communicate with the cytoplasm, a prerequisite for normal cell functioning. As the barrier that separates chromatin from the cytoplasm, the NE is the key regulator that controls the communication between the nucleus and cytoplasm. This communication ranges from macromolecular traffic into and out of the nucleus, mediated by the nuclear pores, to signaling mechanisms with the rest of the cell, mediated by NE-cytoskeleton interactions that link the nucleoplasm and the cytoplasm[2]. The role of cytoskeletal proteins in the regulation of nuclear dynamics has been emerging and now defines a new frontier in Cell Biology[2,5–7]. These nucleoskeleton to cytoskeleton interactions are essential to properly position the nucleus within the cell.

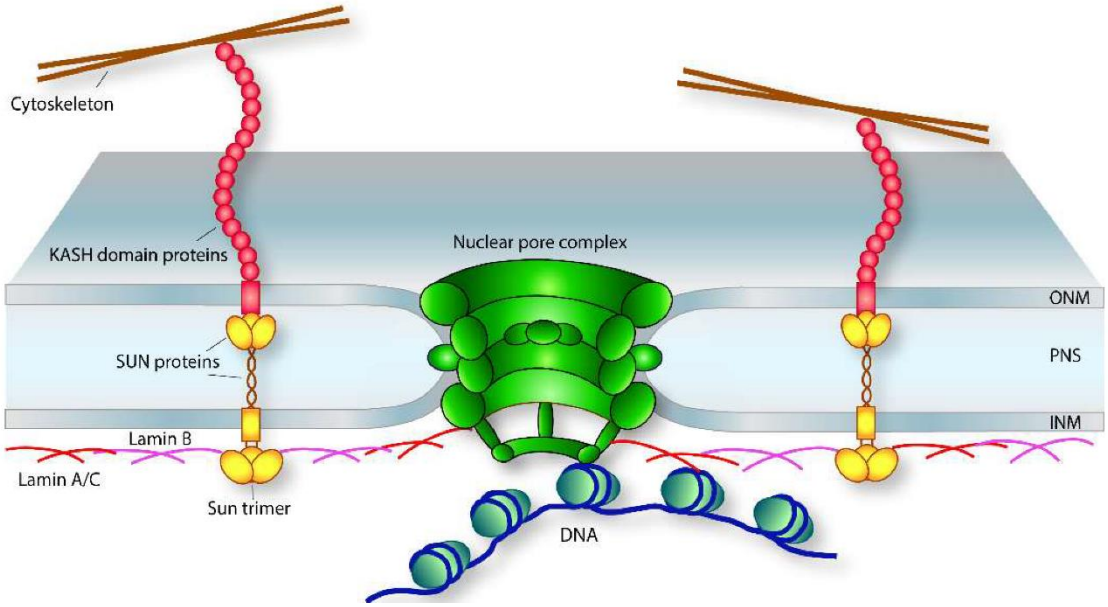

Figure 1.1 Nuclear envelope structure. The communication between the nucleus and the cytoplasm is ensured by macromolecular traffic through the nuclear pore complex and signalling through the coupling between NE (SUN and KASH domain) proteins and the cytoskeleton. This creates a complex communication network where NE proteins, the nuclear lamina and the nuclear pore complex are key regulators of gene expression and cellular responses. Adapted from Preston, C. & Faustino, R. 2018[8].

1.2. Nuclear positioning

Cells actively and precisely position their nucleus within the cytoplasm, being this positioning essential for cell function. Although, the nucleus is commonly depicted in the centre of the cell, it can be asymmetrically positioned depending on cell type, site of cell division, differentiation status and migratory state[9].

Differentiated cells, such as neurons, epithelial cells or myofibers, do not present a centrally located nucleus. Moreover, extreme and crucial nuclear migration events characteristically occur during cell differentiation. In the proliferative zones of vertebrates developing neural structures, the nucleus position along the apical-basal axis varies depending on the stage of the cell cycle in a process known as interkinetic nuclear migration. Here, the nucleus is on the apical side upon entry into G1, moves to the basal side upon progression through G1 and reverses migration toward the apical side upon G2 entrance[10,11]. An analogous nuclear movement occurs in the developing optic epithelium in *Drosophila melanogaster*[12,13]. In myofibers, nuclei are distributed in a large syncytium with several nuclei per cell. Throughout their development, skeletal muscle cells transition from centrally located nuclei (in the myotubes) to periphery positioned nuclei spread out along the myofibers, with specialized regions enriched in nuclei called the neuromuscular junctions[14,15].

During cell division, the nucleus is positioned relative to the plane of division in yeast and fertilized eggs. In the budding yeast *Saccharomyces cerevisiae*, the nucleus must migrate to the bud neck prior to cell division ensuring proper segregation of progeny nuclei. This is known to be promoted by dynein, which localizes to the bud tip and pulls microtubules to drag the nucleus to the bud neck[16]. In turn, to produce two equal daughter cells, the fission yeast *Schizosaccharomyces pombe*, actively positions its nucleus in the centrally located division plane. Here, the nucleus is positioned in the centre of the cell due to antiparallel microtubule bundles with minus ends overlapping at the middle of the cell and plus ends interacting with the cell tips[17]. Another classic example is the pronuclei fusion in fertilized mammalian and invertebrate eggs. Here, prior to the zygote first division, pronuclei must migrate to the cell centre, in a dynein-dependent microtubule-pulling manner, so that after pronuclei fusion and cell division, two equal daughter blastomeres are generated[18]. Here, asymmetric divisions can also take place, although these foresee a previous nuclear movement to the division site[9].

Nuclear positioning assumes a crucial role in proper cell migration, necessary in physiological processes including embryonic development, wound repair, metastasis, neoangiogenesis and tumour invasion. When migrating, cells must pass through narrow openings (frequently smaller than the cell itself) between other cells or in the Extracellular Matrix (ECM), by squeezing the cytoplasmic content[19]. This means that cells will need to repeatedly push and pull the nucleus that must be highly deformed. Hence, being the nucleus both the largest and the stiffest organelle, it limits the ability of cells to migrate through constricted spaces[20]. But the solution for overcoming this limiting step is evidently different between cell types and migration environments.

Generally, to pass the nucleus through constrictions, cells increase the size of the substrate pores by modulating the ECM and/or deform nuclear shape and reduce its stiffness and rigidity by regulating nuclear dynamics[20]. For example, leukocytes position the nucleus close to the protruding front (leading edge) where it can help opening space through the endothelium[21]. On the contrary, most migrating cells, position the nucleus in the rear of the cell, away from the leading edge. Later, cells use different approaches to regulate nuclear dynamics and squeeze it through constrictions, for example, through the relative expression levels between different nuclear lamins, chromatin compactation, actin filaments organization in the nucleoplasm, actomyosin-based contraction in the rear of the nucleus or even by inducing the rupture of the NE followed by NE and DNA repair (using the ESCRT-III machinery)[22–27].

A very particular cell type, neutrophils, optimize the nucleus limiting step by developing increasingly lobulated nuclei and downregulating A-type lamins, allowing the cells to rapidly reach infected sites[28].

Most of the current knowledge on cell migration relies on cells moving on a two-dimensional (2D) substrate, but additional insights are starting to emerge from studies in three-dimensional (3D) environments, that range from micro-fabricated substrates and ECM-derived networks to in tissue preparations, where multiple confinements are applied to the cells[29,30].

1.2.1. The nuclear positioning toolbox

The most well-known processes for nuclear positioning in cell migration come from studies on 2D fibroblast cultures, resorting to wound-healing assays[31,32]. In these, fibroblasts in a starved and wounded monolayer assume a centrally located nucleus prior to migration. After stimulation with serum or the growth factor Lysophosphatidic Acid (LPA), fibroblasts at the wound edge polarize towards the wound before they start to migrate (Figure 1.2)[33]. This polarization creates a leading edge-centrosome-nucleus axis in the direction of migration, with the nucleus being positioned at the rear of the cell, while the centrosome assumes a position between the leading edge and the nucleus (process known as centrosome reorientation)[34]. This axis has also been observed in mesenchymal cells, neurons and most cancer cells[35–37]. Time-lapse microscopy showed that while the centrosome remains anchored near the cell centre, it is the nucleus that actively migrates behind the centrosome in a mechanism dependent on retrograde actin flow mediated by myosin II and the small GTPase Cdc42[33,34,38].

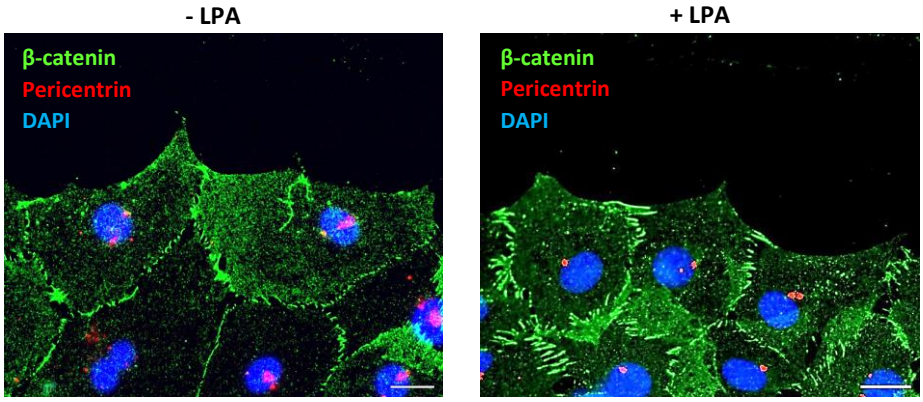

Figure 1.2 Nuclear rearward movement and centrosome reorientation in NIH 3T3 fibroblasts in 2D substrates. The nucleus is centrally located, but upon LPA stimulation, assumes a rearward position in the cell, creating a leading edge-centrosome-nucleus axis. This process was firstly described by Gomes, E.R. *et al.* 2005[33]. Scale bar: 20 μm

To coordinately move and position the nucleus in migrating fibroblasts, it is important to verify two factors. First, the nucleus must be physically connected to the cytoskeleton. Second, mechanical stimuli exerted at the cell surface must be transmitted through the cytoskeleton to the nucleus, where a response may be generated[31]. Thus, to unveil mechanisms of nuclear positioning, it is crucial to understand the nucleoskeleton-cytoskeleton connections.

1.2.1.1. The LINC complex

The physical connection between the nucleus and the cytoskeleton is provided by the Linker of Nucleoskeleton and Cytoskeleton (LINC) complex, composed of ONM Klarsicht/ANC-1/Syne Homology (KASH)-domain proteins and INM Sad1/UNC-84 (SUN)-domain proteins. KASH and SUN proteins physically interact at the perinuclear space, establishing a force transmission channel from the cytoskeleton to the nuclear lamina that is responsible for the final output in the signaling chain[39]. Firstly

described in *Caenorhabditis elegans*, LINC complexes have been identified in all eukaryotic cells[9,40,41].

In mammals, KASH-domain proteins are termed Nesprins and encoded by four (*SYNE*) genes, with the possibility of alternative splicing to generate multiple isoforms. These proteins contain a divergent N-terminal cytoplasmic domain that can interact with different cytoskeleton proteins, thus defining the specificity of the LINC complex: Nesprin-1 and 2 (termed as the "giant" isoforms) bind to actin; Nesprin-3a associates indirectly to intermediate filaments, through plectin; Nesprin-4 binds to microtubules. Conversely, the C-terminus is highly conserved and contains a transmembrane segment that encloses a 10-32 residue KASH domain and spans to the perinuclear space. In fibroblasts, only Nesprin-2 giant (Nesprin-2G) isoform is expressed[39,42,43].

SUN-domain proteins present five isoforms, from which only two, SUN1 and SUN2, are highly expressed. SUN1 and SUN2 bind promiscuously to KASH domains and commonly exist as homotrimers. The N-terminus from SUN-domain proteins is variable and associates with the nuclear lamina. The conserved C-terminal segments reside in the perinuclear space and features coiled-coil regions followed by approximately 200 residues that compose the SUN domain. In fibroblasts, the SUN2 isoform is more expressed than SUN1[39,42,43].

Nesprin and SUN directly bind through their C-terminal KASH and SUN domains at the perinuclear space. This interaction is complex and allows for enhanced force-coupling. Three independent KASH peptides bind to highly organized protomers grooves that constitute the trimeric SUN domain. This interaction is strengthened by a covalent bond between conserved cysteines on both domains[42]. A recent study showed that this disulfide bond is necessary for the maximal force transmission by the LINC complex *in silico*[39].

1.2.1.2. The cytoskeleton

Positioning the nucleus greatly depends on the capacity of the cytoskeleton to generate forces and on the sum of all those forces applied on the nucleus. If there are no forces acting or the sum of all acting forces is zero, the nucleus assumes a stationary position, whether its centred in the cell or not[44]. Recent studies indicated that even when the nucleus is stationary, it is always under cytoskeletal forces[45–47]. One of the clearest examples of dynamic forces continuously applied to the nucleus comes from Zhu and colleagues. It was shown that, after displacing nuclei using centrifugal force, multiple cytoskeletal forces were exerted to rapidly recentre nuclei[47]. Thus, when the forces applied on the nucleus are unbalanced, the nucleus moves, but only until a new balance of forces is established, assuming a new stationary position. To displace the nucleus in migrating fibroblasts, a threshold of cytoskeleton force on the order of tens of nN needs to be applied[48]. But what are the cytoskeletal components that generate such forces? Depending on the cell type, all three cytoskeleton components, microtubules, intermediate filaments or actin filaments can work separately or as a set to position the nucleus. Most nuclear movements described are mediated through microtubules. Although, a growing number of actin-mediated movements has been described and gained significant relevance in fibroblasts' cell migration[9,49].

Actin is an ATP-binding protein that exists in the cell in two forms: G-actin, a single polypeptide chain with a globular configuration, and F-actin, the filamentous polymer composed by G-actin monomers. As a cytoskeletal protein, actin organizes the cell cortex either by facilitating traffic at the plasma membrane or by mediating cell-shape changes[50]. Regarding its functions in nuclear positioning, it has been shown that, upon LPA stimulation in fibroblasts, an irregular actin meshwork formed near the nucleus rearranges itself, in an myosin II dependent manner, to form cables on the dorsal surfaces of the cell that orient parallel to the leading edge[33,50]. These dorsal actin cables integrate a retrograde actin flow and stablish a direct connection with Nesprin-2G from the LINC complex, resulting in the displacement

of the nucleus to its rearward position. The coupling of Nesprin-2G and SUN2 to actin dorsal cables leads to linear arrays of NE proteins, defining a new structure: Transmembrane Actin-associated Nuclear (TAN) lines (Figure 1.3)[38,51]. Although LINC complex proteins assemble TAN lines, other proteins have been identified as regulators of LINC complex for TAN lines formation and dynamics. It has been described that NE proteins Samp1 and AAA+ TorsinA (with its activator LAP1) promote stability and anchorage for TAN lines, while cytoskeletal actin-interacting proteins formin FHOD1 and Fascin promote the anchorage of moving dorsal actin cables to the LINC complex[52–55].

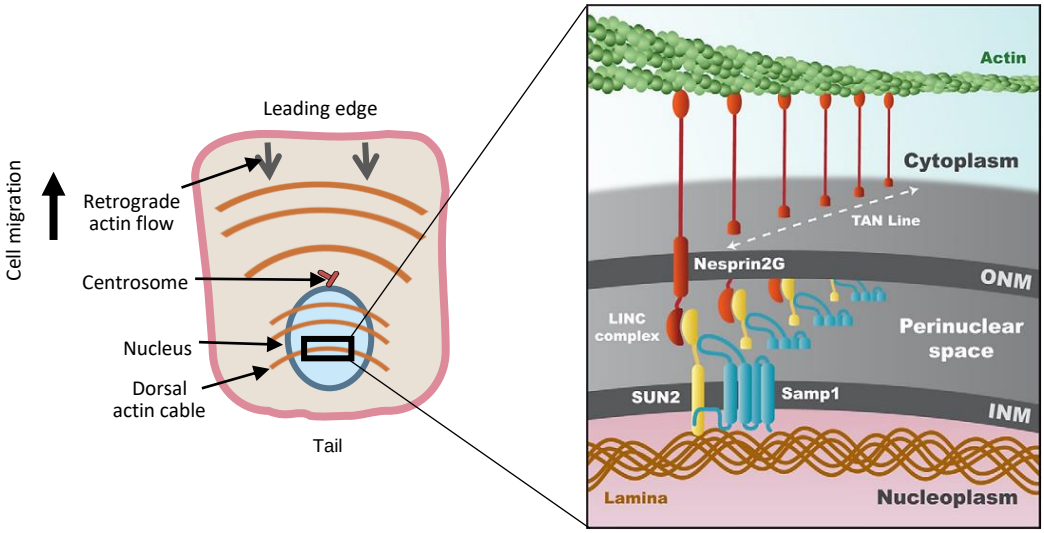

Figure 1.3 Cytoskeleton-nucleoskeleton coupling through TAN lines. These lines are composed of LINC complex proteins (Nesprin-2G and SUN2) that assemble into linear arrays through the NE surface and can connect to actin cables. Other proteins, such as Samp1, have been reported to assist TAN lines formation and dynamics. Adapted from Borrego-Pinto, J. *et al.* 2012[52].

1.2.2. Nuclear mispositioning and disease

Given that nuclei are positioned for specialized cellular functions, it can be presumed that abnormalities in the molecular toolbox underlying nuclear positioning lead to dysfunction and pathology. However, in many cases, it is not clear how nuclear positioning defects contribute to disease or why it only compromises cells in specific tissues[9].

Over 400 mutations in the *LMNA* gene (that encodes for lamins A/C) have been described and associated with various disease phenotypes termed laminopathies[56,57]. These range from multi-organ to tissue-specific diseases, frequently overlapping in the same patient[57–59]. More particularly, migrating fibroblasts depleted of A-type lamins, do not present rearward nuclear movement. Instead, Nesprin-2G assembles into TAN lines that slip over the nucleus due to a lamin-dependent anchorage defect[60].

In cancer, deregulation of nuclear position and deformation are directly linked to the malignant transformation and metastatic potential of cells. Intensive research has been focusing on lamins expression levels as markers for development and progression of different tumors, such as breast, lung or prostate cancers[61–64].

Centrally located nuclei are present in different myopathies, such as Epidermolysis Bullosa Simplex with Muscular Dystrophy (caused by the deficiency in plectin, a cytoskeleton linker), desminopathies (caused by deficiencies in intermediate filament desmin) or Centronuclear Myopathy (with variable genetic forms such as mutations in membrane-related genes *DNM2* or *MTM1*)[65–67]. These and several other myopathies have also been correlated with mutations in *SUN*, *SYNE* and *LMNA* genes[59,68].

Mutations in SUN- or KASH-domain proteins coding sequences have also been linked to other diseases. For example, mutations in *SYNE1* are associated to neurodegenerative diseases such as Autosomal Recessive Cerebellar Ataxia type 1[59]. In columnar epithelia, more specifically in hair cells at the inner ear, knockouts of either Nesprin-4 or SUN1 resulted in mispositioning of nuclei in inner hair cells and hearing loss of high frequencies[31]. In spermiogenesis, SUN4 knockout has been correlated with cytoskeleton disorganization and lack of nucleus elongation, which resulted in associated infertility[69].

Apart from disease, it is also accepted that abnormal nuclear shape and positioning may contribute to the normal aging process. This has been reported in *C. elegans* nonneural cells and in fibroblasts from individuals over 60 years old[70,71].

1.3. Searching for new players

Previously in Gomes lab, two new players were identified, involved in nuclear movement in migrating fibroblasts: the C-Terminal Domain Nuclear Envelope Phosphatase 1 (Ctdnep1) and the Epidermal Growth Factor Receptor Kinase Substrate 8-Like Protein 2 (Eps8L2).

1.3.1. Ctdnep1

Ctdnep1 (previously termed Dullard) is a 244 amino acid (28,4 kDa) protein with serine/threonine phosphatase activity. This is a transmembrane protein that localizes at the nuclear envelope and the endoplasmic reticulum (ER)[72]. Structurally, Ctdnep1 is known to have a N-terminal transmembrane (TM) domain, and a C-terminal FCP1 homology domain (responsible for Ctdnep1 phosphatase activity) (Figure 1.4)[73].

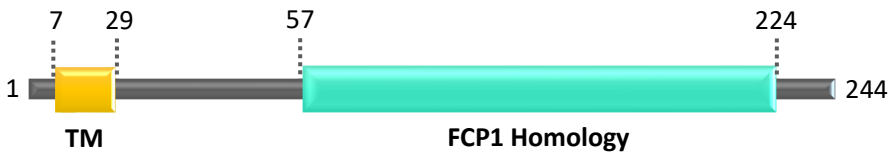

Figure 1.4 Schematic representation of the human Ctdnep1 protein. In 244 amino acids, this protein comprises a transmembrane domain and a FCP1 homology domain with a characteristic DXDX(T/V) catalytic motif.

Ctdnep1 was firstly described for its role in early neural tube development in *Xenopus laevis*[72]. Later this neural induction role was correlated with the negative regulation of Bone Morphogenic Protein (BMP) signaling by Ctdnep1[74]. This role is now believed to be tissue specific[73,75]. Additionally, Ctdnep1 functions as an agonist of WNT signaling during germ cell specification in mouse embryos[75]. Although, Ctdnep1 is most known for dephosphorylating and, consequently, activating, the mammalian phosphatidate phosphatases Lipin-1 and -2, in the presence of the Nuclear Envelope Phosphatase 1-Regulatory subunit 1 (Nep1-r1)[76]. Lipin activation is particularly important for the biogenesis of nucleus and ER membranes as Lipin catalyzes the conversion of phosphatidic acid to diacylglycerol and controls the overall fatty acids metabolism[73,76,77]. In disease, Ctdnep1 truncated forms have been associated with medulloblastoma, the most common malignant pediatric brain tumor[78,79]. Moreover, unlike most brain tumours, medulloblastoma frequently metastasize[80].

1.3.2. Eps8L2

Eps8L2 is a cytoskeletal actin regulator protein of the Eps8-related proteins family. Its amino acid chain has 715 residues (80,6 kDa) and is composed, at the N-terminus, by Phosphotyrosine Binding (PTB) and Epidermal Growth Factor Receptor (EGFR) domains and, at the C-terminus, by Src Homology 3 (SH3) and F-actin binding domains (Figure 1.5)[81].

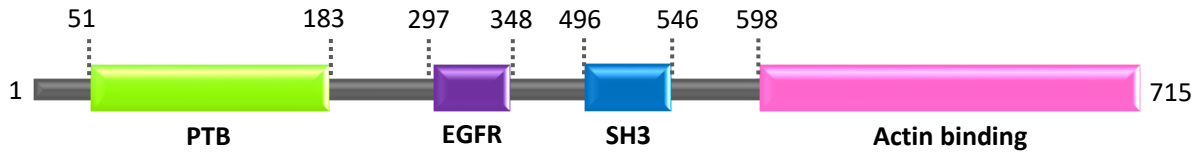

Figure 1.5 Schematic representation of the human Eps8L2 protein. Its 715 amino acid chain contains a PTB domain, an EGFR domain, a SH3 domain and an actin binding domain ("effector region") with both capping and bundling activities.

Eps8L2 is most known for its role in the Sos1-Abi1-PI3K-Eps8L2 complex. Within the complex, Abi1 acts as a scaffold, on which Eps8L2, PI3K and Sos1 assemble to stimulate Sos1 Guanine Nucleotide Exchange Factor (GEF) activity, leading to small GTPase Rac activation and, therefore, cytoskeletal remodelling. Consistently, it was shown that Eps8L2 could localize at F-actin-rich membrane ruffles and rescue actin remodelling in Eps8 -/- fibroblasts[81]. Moreover, Eps8L2 acts as an actin dynamics regulator by presenting actin capping and bundling activities[82]. By capping actin barbed ends, Eps8L2 limits the growth of actin filaments[83]. By bundling actin filaments, Eps8L2 can generate stiff rods capable of enduring greater mechanical stimuli in the cell[84]. More recently, Eps8L2 was described in mouse and human cochlea, where it is required for stereocilia maintenance through actin bundles organization in adult hair cells. In these cells, Eps8L2 knockout leads to progressive hearing loss due to progressive structural disorganization of the hair bundles[85]. In cancer, Eps8L2 presents 4 folds higher expression in meningiomas, the most frequent primary intracranial tumor[86].

1.3.3. Previous work

Nuclear positioning in starved cells is typically around -5% from the cell centroid (% of the cell radius), which is coincident to a somewhat centred location in the cell (cell centre = 0). Upon LPA stimulation, the nucleus is positioned at around -20% relative to the cell centroid, thus it becomes positioned at the cell rear. On the other hand, the centrosome is reoriented if it is located between the leading edge and the nucleus. Starved cells typically present a centrosome reorientation of 40%, which is considered a basal centrosome reorientation state. Upon LPA stimulation, centrosome reorientation is around 60%. Thus, a protein is involved in nuclear movement if, in its absence, the nucleus positioning and the centrosome reorientation is proximal to the levels of non-stimulated cells[33,34]. Previously in Gomes lab, at Instituto de Medicina Molecular João Lobo Antunes, it was observed that, upon knockdown of Ctdnep1 or Eps8L2, nuclear positioning and centrosome reorientation were significantly impaired in NIH 3T3 cells, presenting values closer to the unstimulated Control. Ctdnep1 and Eps8L2 knockdown cells presented between approximately 5% to 10% of nucleus displacement, with only around 40% of cells presenting centrosome reorientation[87].

When studying the possible interaction between Ctdnep1 and Eps8L2, it was observed that these proteins interacted physically and directly with each other[87]. Additionally, when depleting either of these proteins, the percentage of cells with TAN lines and the number of TAN lines per cell were decreased[87]. The absence of Ctdnep1 or Eps8L2 also led to a decrease in thickness of dorsal actin cables[87].

Overall, these results identified two new players in nuclear positioning: Ctdnep1 and Eps8L2. These proteins were shown to physically and directly interact to regulate dorsal actin cables organization and, thus, be important for TAN line-dependent nuclear positioning in migrating fibroblasts. But how the interaction between Ctdnep1 and Eps8L2 is coupled to nuclear positioning is not yet fully explored. This will be the focus of the present thesis.

2. Aims of study

Three main aims were outlined for this work:

1. Study Ctdnep1 and Eps8L2 subcellular localization in migrating fibroblasts and check if these proteins colocalize with each other;
2. Analyse Eps8L2 dephosphorylation by Ctdnep1 as a potential underlying mechanism mediating their interaction;
3. Determine the role of Ctdnep1 and Eps8L2 in cell migration.

3. Materials and methods

3.1. Cell culture and transfections

NIH 3T3 cells were cultured in Dulbecco's Modified Eagle Medium (DMEM) without sodium pyruvate (Gibco™ #41965039) supplemented with 10% bovine calf serum (Corning #35-053-CM), 10 mM HEPES (Gibco™ #15630056) and 500 units/mL penicillin and streptomycin (Gibco™ #15140122).

U2OS cells were cultured in DMEM with sodium pyruvate (Gibco™ #41966029) with 10% fetal bovine serum (Eurobio ingen #CVFSVF00-01) and 500 units/mL penicillin and streptomycin (Gibco™ #15140122).

HEK 293 cells were cultured in DMEM with sodium pyruvate with 10% fetal bovine serum.

All cell lines were split at a maximum confluence of 80% with TrypLE™ Express Enzyme (Gibco™ #12605028). Cells were grown at 37 ºC with 5% CO_2 saturation in a humidified incubator.

3.1.1. Plasmid transfections

3.1.1.1. NIH 3T3

NIH 3T3 cells were electroporated with plasmid DNA using Cell Line Nucleofector™ kit R (Lonza #VCA-1001) and Nucleofector™ 2b Device (Lonza #AAB-1001), following the manufacturer's recommendations. For each electroporation, 1 x 10^6 cells in Nucleofector® solution were combined with 5 µg DNA. Immediately after pulsing, cells were recovered in pre-equilibrated culture medium and incubated at 37 ºC with 5% CO_2. 48 h post-electroporation, drug selection media with 2,5 µg/mL puromycin (Sigma-Aldrich #P8833) or 1,5 mg/mL G418 (InvivoGen #ant-gn-1) was added to select for the positively transfected cells. Wild-type (WT), non-transfected, cells were used as a control for the drug selection. All control cells died after approximately 4 days of puromycin selection or 7 days of G418 selection. At this point, positively transfected cells were enriched in two rounds of FACS.

3.1.1.2. U20S

U20S cells were transfected with plasmid DNA using Lipofectamine™ 3000 (ThermoFisher Scientific #L3000008) in a P100 mm dish format, following the manufacturer's recommendations. Briefly, 2 µg of plasmid DNA were diluted in OPTI-MEM™ I medium (Gibco™ #31985-047) and incubated with Lipofectamine and P3000 reagent for 20 min at Room Temperature (RT). DNA-Lipofectamine complexes were then added to previously seeded cells (to an approximately 80% confluence). Cells were incubated at 37 ºC with 5% CO_2 for 24 h. Then, cells were lysed by scrapping the dish bottom with 500 µL of cold lysis buffer with the following composition: 25 mM Tris-HCl pH 8, 100 mM NaCl, 1% Triton X-100, 10% glycerol, 1x cOmplete™, EDTA-free Protease Inhibitor Cocktail (Roche #04693132001) in PBS, 1x PhosSTOP™ (Sigma-Aldrich #04906837001) in PBS and Milli-Q water. For samples that would undergo lambda phosphatase treatment, lysis was carried out without the phosphatase inhibitor (PhosSTOP™). Cell extracts were incubated on ice for 30 min, centrifuged at 13,3 rpm at 4 ºC for 20 min and the supernatants (with total cell lysate) were stored at -80 ºC until Western blot or immunoprecipitation was performed.

All plasmids used for NIH 3T3 or U2OS transfections are indicated in Supplementary Table 7.1.

3.1.2. Reverse siRNA transfections and wound-healing assays

For analysis of cell migration, wound-healing assays were performed. In these, cells were transfected using Lipofectamine RNAiMAX (Invitrogen #13778150) in a 6-well plate format, following the manufacturer's recommendations. Briefly, the siRNA was diluted in OPTI-MEM™ I medium (Gibco™ #31985-047) and Lipofectamine was added. After 15 min of incubation at RT, the mixture was added to a 22 x 22 mm coverslip. A cell suspension was then added to an approximately 20% confluence. At 48 h post-transfection, cells were washed 4 times in serum free culture medium and starved for another 48 h. After grown to confluency, cells were wounded with a pipette tip and stimulated with complete culture medium. Imaging of wound closure was then performed, acquiring 6 positions per coverslip every 15 min for a course of 16 h. Wound closure area was quantified by measuring the wound area at 0 h and after 16 h, using the Fiji software[88] with the Multi-Template Matching plugin[89].

The following siRNAs were used: Silencer™ Select Negative Control No. 1 (Invitrogen #4390843); Silencer™ Select Ctdnep1 siRNA mouse 5'-GAUUCACUCUCACCACGAUtt-3' (Ambion #4390771/s205755); Silencer™ Select Eps8L2 siRNA mouse 5'-GCAGGUGAACGACAAGUCAtt-3' (Ambion #4390771/s97342). All siRNAs were used at a final concentration of 500 nM.

For analysing nuclear positioning in NIH 3T3 transfected cells or in the knockout Eps8L2 clones, no siRNA transfection was performed. Cells were grown in glass coverslips and wounded monolayers were stimulated after starvation with 20 µM LPA for 2 h, as described before[33,90–92]. Coverslips were then fixed and immunostained. For nucleus and centrosome positioning assessment, ideally, more than 50 cells at the wound edge were quantified (per coverslip), using the Cell Plot software[93]. Centrosome reorientation was analysed in the same cells quantified for nucleus and centrosome positioning.

3.2. CRISPR/Cas9

Individual lentiviral CRISPR/Cas9 plasmids targeting a single genomic locus in endogenous *CTDNEP1* or *EPS8L2* sequences were generated as previously described[94,95]. For *CTDNEP1*, the guide RNA (gRNA) targeted a sequence near the stop codon, while for *EPS8L2* a region near the start codon was targeted. Briefly, 2 oligonucleotides (20 bp) were designed to target a single *CTDNEP1* or *EPS8L2* genomic locus and flanked on the 3' end by a NGG Protospacer Adjacent Motif (PAM) sequence, using the CRISPOR software[96] (Supplementary Table 7.2). The oligonucleotides were annealed with T4 Polynucleotide Kinase (New England Biolabs #M0201S) in T4 DNA Ligation Buffer (New England Biolabs #B0202S). Then, using T4 DNA Ligase (Takara #2011A), the oligo duplex was cloned into LentiCRISPR v2 vector (Addgene #52961) previously digested with BsmBI (New England Biolabs #R0580S). Transformation was performed into Stbl3™ Chemically competent *Escherichia coli* (Invitrogen #C737303), according to the manufacturer's recommendations.

To produce lentivirus, the cloned LentiCRISPR v2 plasmid was co-transfected into HEK 293 cells with the packaging plasmid Delta 8.9 and envelope construct VSV-G (both plasmids were gifts from Olivier Pertz, University of Basel), using Lipofectamine 3000 according to the manufacturer's recommendations. After 48 h of virus production, the cell culture supernatant was harvested, filtered (through a 0,45 µm pore) and centrifuged at 25 000 rpm for 90 min at RT. The virus pellet was then re-suspended in 100 µL sterile PBS and stored at -80 ºC until further usage.

For the virus infection, 10 µL lentivirus aliquot and 8 µg/mL hexadimethrine bromide (Sigma-Aldrich #H9268) were added to previously seeded NIH 3T3 cells (to an approximately 30% confluence). Infection was carried out for 24 h at 37 ºC with 5% CO_2. 48 h post-infection, 2,5 µg/mL puromycin was added to select for cells expressing LentiCRISPR v2 sequences.

3.2.1. Knockin

To tag the endogenous Ctdnep1 or Eps8L2, the DNA template (Figure 3.1A and B) was inserted through electroporation and, approximately 8 h post-electroporation, lentiviral infection was carried out as mentioned above (section 3.2). After expansion in culture for up to 1 week with drug selective media, GFP- or miRFP670-positive cells were selected through FACS. Screening for positively tagged cells was conducted through microscope observation.

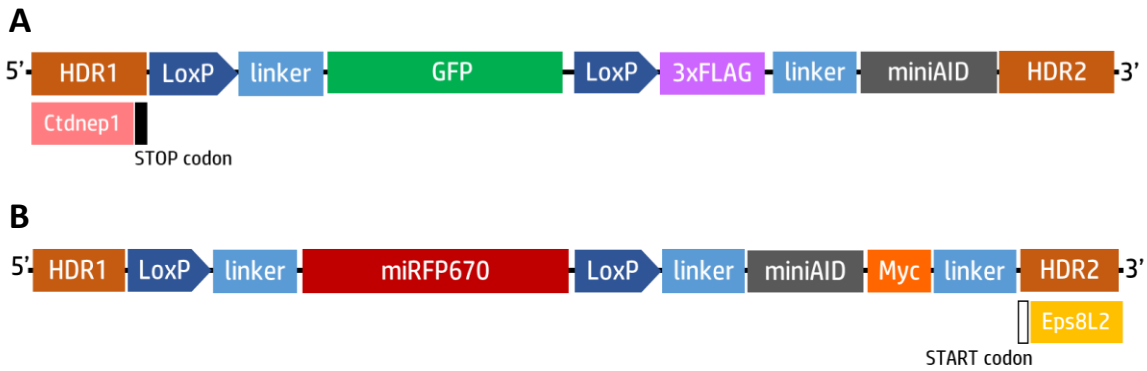

Figure 3.1 (A, B) Schematic representation of the template DNA used for tagging the endogenous Ctdnep1 or Eps8L2, respectively, in the CRISPR/Cas9 knockin assays.

3.2.2. gRNA validation and knockout generation

For gRNA validation or generation of knockouts for Eps8L2, lentiviral infection and drug selection were performed as mentioned above (section 3.2). After expansion in culture for up to 1 week, FACS for single-cell cloning was performed in a 96-well format.

FACS plates were scanned for monoclonal population wells and 15 (for validation of the gRNAs) or 60 (for generation of Eps8L2 knockout cell lines) selected clones that met this criterion were expanded to larger culture dishes until the P100 mm or 12-well plate formats, respectively. At this point, genomic DNA was extracted with NZY Tissue gDNA Isolation kit (NZYTech #MB135), following the manufacturer's instructions. Then, Polymerase Chain Reaction (PCR) amplification of the theoretical Cas9 target site and flanking regions was performed. For the amplification reactions, 50 ng of genomic DNA from each clone and from WT, non-transfected, cells were amplified using Q5® High-Fidelity DNA Polymerase (New England Biolabs #M0491L) for Eps8L2 assays or NZYTaq II 2x Green Master Mix (NZYTech #MB358) for Ctdnep1 assay, according to the respective manufacturer's instructions. Primers sequences and amplicons size used are indicated in Supplementary Table 7.3. Amplicons were analized through a 2% agarose gel in 1x TBE buffer pH 8,3, using NZYDNA Ladder VI (NZYTech #MB089) as a marker for amplicon size. Amplicon bands were isolated from the gel and DNA was purified using QIAquick Gel Extraction kit (Qiagen #28704), following the manufacturer's instructions. DNA yield was determined using Nanodrop 2000 apparatus. Purified DNA was sequenced using Sanger sequencing services from GATC and analysed through the SnapGene 2.8.2 software[97].

3.3. FACS

NIH 3T3 cells were trypsinized, centrifuged at 800 rpm for 5 min at RT and the cell pellet was resuspended in sorting media with the following composition: 1x PBS, 5% bovine calf serum, 0,5 µg/mL amphotericin B (Sigma-Aldrich #A2942) and 0,1 mg/mL gentamicin (Gibco™ #15750037). Cells were then filtered through a 70 µm cell strainer to 5 mL sorting tubes.

Sorting was performed at the Flow Cytometry facility at Instituto de Medicina Molecular João Lobo Antunes, using a BD FACSAria III housed in a Baker BioProtect-IV bio-safety cabinet set to 4 ºC and equipped with blue (488 nm), yellow-green (561 nm) and red (633 nm) lasers controlled by FACSDiva™ 6.1.3 software. For sorting NIH 3T3 cells, a 100 µm nozzle was used. To exclude dead cells from gated populations, near infrared live/dead staining (Invitrogen #L34975) for excitation at 633 nm was performed. To exclude cells without GFP expression, control, non-transfected cells were analysed in the sorter. For single-cell cloning experiments, live cells were selected to compose the gated population. To sort NIH 3T3 cells transfected with Ctdnep1, Ctdnep1_D67E or Eps8L2 plasmids, GFP positive cells composed the gated populations.

After FACS, cells were grown in previously filtered (through a 0,45 µm pore) conditioned medium (collected from NIH 3T3 WT cells with the same medium for 2 days in culture) mixed in a 1:1 proportion with fresh complete medium, 0,5 µg/mL amphotericin B (Sigma-Aldrich #A2942) and 0,1 mg/mL gentamicin (Gibco™ #15750037).

3.4. Immunofluorescence

Cells were fixed immediately after aspiration of media with 4% paraformaldehyde (Science Services #E15711) in PBS for 10 min at RT, washed with PBS and permeabilized with 0,3% Triton X-100 in PBS for 5 min. Blocking and primary antibody incubation was performed simultaneously. Primary and secondary antibodies, phalloidin and DAPI were diluted in PBS containing 10% goat serum (Sigma-Aldrich #G9023) and incubated with the cells in a humid chamber for 1 h at RT. After antibodies incubations, coverslips were washed 3 times, for 20 min each, with PBS. Coverslips were mounted in Fluoromount-G™ (Invitrogen #00-4958-02). All antibodies and dyes used are indicated in Supplementary Table 7.4.

3.5. Cell imaging

All images were acquired using a Zeiss Axio Observer widefield inverted microscope equipped with a sCMOS camera Hamamatsu ORCA-flash4.0 V2 controlled by ZEN Blue Edition software. For visualization of GFP expression pattern in NIH 3T3 transfected cells, a 63x/1,4 Plan-Apochromat DIC M27 oil objective was used. For nuclear positioning analysis, an EC Plan-Neofluar 40x/1,30 Ph3 M27 oil objective was used. For time-lapse imaging, a chamber at 37 ºC with 5% CO_2 and an EC Plan-Neofluar 10x/0,30 Ph1 M27 objective were used.

3.6. Western blotting

For lambda phosphatase treatment, 40 µL of total lysate was added to 400 U of lambda phosphatase (New England Biolabs #P0753S) in 1x NEBuffer for Protein MetalloPhosphatases, supplemented with 1 mM $MnCl_2$, and incubated at 30 ºC for 30 min. Reactions were stopped by addition of 1x SDS Sample Buffer (Millipore #70607) and incubation at 98 ºC for 5 min.

Total cell lysates, previously resuspended in SDS sample buffer and boiled, were loaded (15 µL of lysate per lane) and resolved on 4-15% Mini-PROTEAN® TGX™ Precast protein gels (Bio-Rad #4561026). Transfer was performed into nitrocellulose membranes (Millipore #HATF00010), using the Mini Trans-Blot® Cell wet transfer system (Bio-Rad #1703930). As a molecular weight marker, NZYColour Protein Marker II (NZYTech #MB090) was used. Membranes were blocked using 5% w/v non-fat milk in TBS with 0,1% Tween® 20 (TBST) for at least 30 min at RT. Western blots were probed overnight at 4 ºC with the primary antibodies diluted in blocking solution (Supplementary Table 7.4). After

washing membranes with TBST (3 times wash, 20 min each), these were incubated with the corresponding secondary antibodies (diluted in blocking solution) for 90 min at RT (Supplementary Table 7.4). After washing membranes as before, these were developed using Amersham ECL Prime detection reagent (GE Healthcare #RPN2232). ChemiDoc XRS+ system (Bio-Rad) was used for image generation.

3.7. Immunoprecipitation and mass spectrometry

To analyse the phosphorylation sites in Eps8L2, U2OS cells were transfected with Myc-Eps8L2 or co-transfected with Myc-Eps8L2 and Ctdnep1-GFP or Ctdnep1_D67E-GFP, with or without Nep1-r1-HA-ProtA. All lysates were immunoprecipitated for Myc-Eps8L2.

For immunoprecipitations, 500 µL of cell lysate were precleared with 20 µL Halo-Trap agarose beads (Chromotek #ota-20), previously washed with PBS, and the mixture was incubated at 4 ºC in agitation for 30 min. After centrifuging at 13 300 rpm for 5 min at RT, cell lysates were harvested and mixed with 50 µL Myc-Trap®_A agarose beads (Chromotek #yta-20) previously washed two times with PBS and once with lysis buffer. After incubation at 4 ºC in rotation for 2 h, beads were washed 3 times with wash buffer (125 mM Tris-HCl pH 8, 150 mM NaCl and Milli-Q water). Then, the supernatant was completely removed, and beads were incubated with 1x SDS Sample Buffer at 98 ºC for 5 min. Samples were then analysed through Western blot and mass spectrometry.

Three independent transfections and immunoprecipitations were performed for each condition and sent to tandem mass spectrometry analysis at the Proteomics Core Facility at the European Molecular Biology Laboratory (Heidelberg, Germany). There, samples were individually labelled with tandem mass tags and prepared for identification and quantification of Eps8L2 phosphoresidues, as previously described[98].

3.8. Data analysis

All quantifications are presented as mean ± Standard Error of the Mean (SEM) of at least three independent replicates per experiment to ensure reproducibility. In wound-healing assays for *EPS8L2* knockout screening, data from one or two independent replicates is represented. Data representation and statistical significance between groups were assessed through unpaired Student's *t*-tests using the GraphPad Prism 8.2.1 software[99]. A probability $P<0,05$ was considered statistically significant.

4. Results and discussion

4.1. Ctdnep1 and Eps8L2 subcellular localization

Ctdnep1, a NE and ER phosphatase[73], and Eps8L2, a cytoskeletal actin regulator protein[81], were previously shown to physically and directly interact and be determinant for nuclear positioning in migrating fibroblasts. But where this interaction takes place in the cell or if Ctdnep1 and Eps8L2 subcellular localization affect one another, has not yet been explored. To study Ctdnep1 and Eps8L2 subcellular localization, the most straightforward approach would consist in performing immunocytochemistry. However, considering that there are no suitable antibodies for the endogenous proteins, cell lines expressing tagged versions of Ctdnep1 and Eps8L2 were generated.

Tagging the endogenous proteins through CRISPR/Cas9 knockin assays would provide data closest to the physiological expression levels and localization. Electroporation was performed to insert a plasmid coding for the tag sequence and lentiviral infection to insert the coding sequences for the Cas9 and gRNA. In this system, the gRNA binds to the cell's DNA based on sequence complementarity and acts as a scaffold sequence for Cas9, consequently defining the genomic target to be modified. In turn, Cas 9 performs a Double-Strand Break (DSB) in the DNA upstream of a PAM sequence[100]. The DSB can then be resolved by Homology-Directed Repair (HDR) using the DNA template initially electroporated, resulting in the insertion of the tag sequence in the target DNA.

For Ctdnep1, the stop codon region was tagged to insert a GFP/FLAG tag, since previous data suggested that tagging the N-terminus could affect Ctdnep1 function. For Eps8L2, the start codon was tagged to insert a miRFP670/Myc tag, thus excluding the possibility of affecting the C-terminus actin-binding domain-related functions. FACS was performed to enrich the cell population in GFP- or miRFP670-positive cells. Although between 1000 and 2000 positive cells were gated for each knockin assay, no positive cells were observed under the microscope and an extensive cell death was frequently noted after a short period in culture. Additionally, performing a second FACS did not enrich the number of positive cells. Altogether, these observations point out that either all positively tagged cells died after FACS or that the gated population was composed of false positives.

To test if the Cas9 was not cutting the target sequence in the current system and thus cells were not presenting the desired edit, NIH 3T3 cells were infected with the Cas9 and gRNAs coding sequences to perform the DSB and induce repair. Since, in this case, no DNA template was inserted, the repair would likely be performed by the Non-Homologous End Joining (NHEJ) pathway, resulting in variable Insertions or Deletions (INDELs) at the DSB. To screen for mutations in *CTDNEP1* or *EPS8L2* sequences, amplification of the target sequence and flanking regions in the genomic DNA from 15 selected single-clones was performed. Ctdnep1 clone 6 presented a band with higher electrophoretic mobility compared to the WT control, indicating possible mutations (Figure 4.1A). No band shift for Eps8L2 clones was observed (Figure 4.1B). To obtain a more sensitive detection of the mutations, the amplicon with higher electrophoretic mobility in Ctdnep1 clone 6 and amplicons from all Eps8L2 clones were sequenced. When analysing the DNA sequences from Ctdnep1 and Eps8L2 clones, deletions and point mutations were observed in the target region (Figure 4.1C and D, respectively), indicating that the gRNAs used were recognizing the desired sequence and the Cas9 was indeed cutting.

Another important factor should be considered when assessing the limiting step in the knockin approach: the low efficiency of HDR. In mammals, HDR is rarely used to resolve DSB and this repair is restricted to S and G2 phases of the cell cycle, with NHEJ bearing the major proportion of DNA repairs and being active in all stages of the cell cycle[100]. Thus, to tilt the repair pathway choice in favour of HDR, several

changes in the knockin approach could be tested, such as the use of chemical or genetic inhibitors of key enzymes involved in NHEJ, the synchronization of cells in S and G2 or the use of modified Cas9 (for example through binding to CtIP, a protein essential for HDR initiation)[101–103]. Additionally, positioning the template DNA near the target site, by covalent binding to the Cas9, has been shown to increase the HDR pathway efficiency[104].

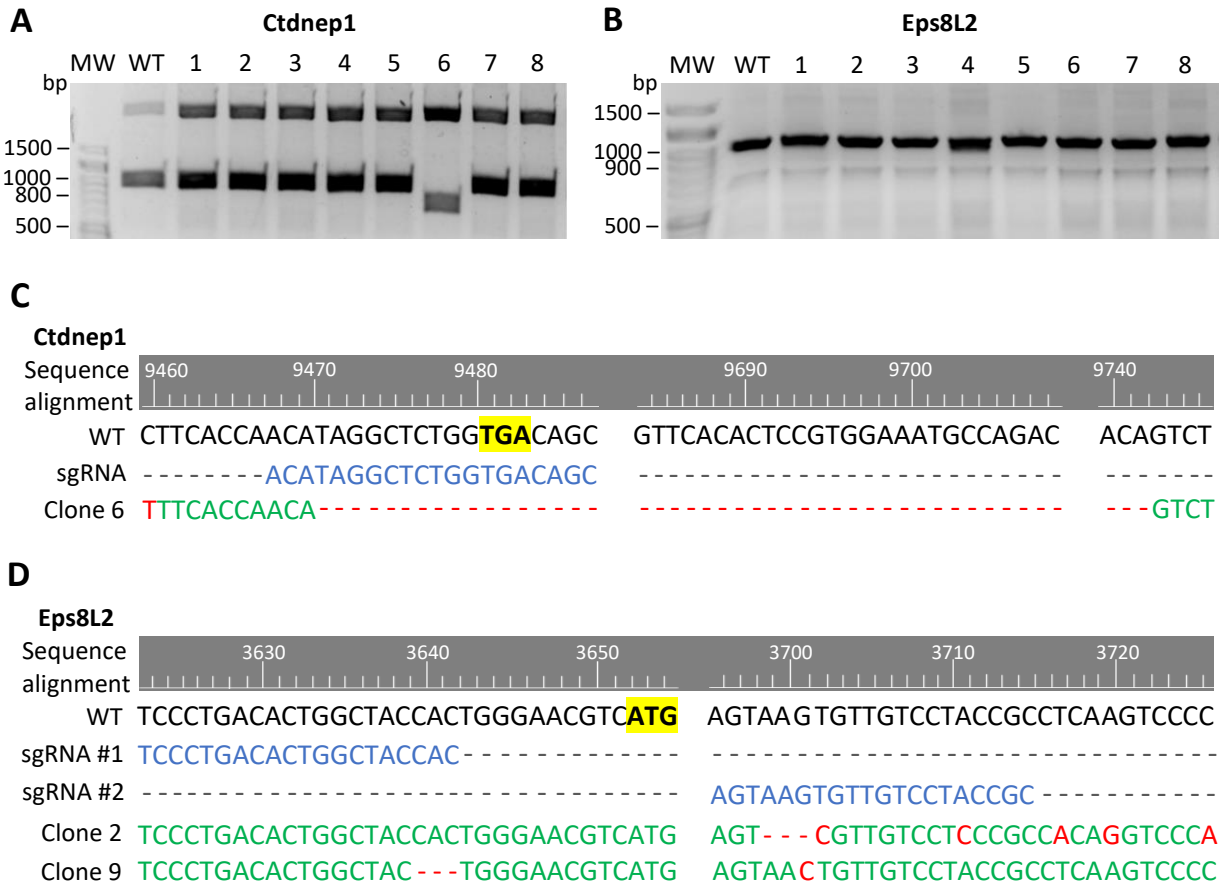

Figure 4.1 Validation of the gRNAs used in Eps8L2 and Ctdnep1 knockin assays. (A, B) Agarose electrophoresis for 8 representative Ctdnep1 or Eps8L2 clones, respectively (each identified with a number). As a reference, WT (non-transduced) cells, were used. In all cases, an amplicon of approximately 1000 bp is expected for a non-mutated sequence. MW: molecular weight marker. **(C, D)** Alignment between genomic DNA sequences for Ctdnep1 clone 6 or Eps8L2 clones 2 and 9, respectively, and the WT sequence. For Eps8L2 assay, two gRNAs were used, while for Ctdnep1 assay, only one gRNA was used. The position of each nucleotide indicated was determined using the correspondent NCBI reference sequence (NC_000077.5 for Ctdnep1 and NC_000073.6 for Eps8L2). gRNAs are marked as blue, matching regions as green and mismatching regions as red. Start (ATG) and stop (TGA) codons are highlighted in yellow in the respective WT sequences.

Knockout of cells for *EPS8L2* or *CTDNEP1* using the CRISPR/Cas9 approach was also attempted. These cell lines would allow to analyse the impact of the full absence of these proteins during nuclear movement (since previously only data relative to knockdown experiments was obtained). It would also be interesting to insert an Eps8L2 tagged construct in a Ctdnep1 knockout cell line (or vice versa) and further investigate if Eps8L2 or Ctdnep1 subcellular localization changes in the absence of its binding partner and even test if the introduction of Eps8L2 or Ctdnep1 in the knockout cell lines would rescue the nuclear positioning phenotype.

Regarding *CTDNEP1*, using the current gRNA, a complete knockout will be challenging given the fact that the stop codon is being targeted and, thus, the probability of obtaining truncated, but entirely (or at least partially) functional versions of Ctdnep1, is very high. Thus, a new gRNA targeting the start codon region was designed and screening for knockout clones is ongoing.

For *EPS8L2*, since a validated gRNA targeting the gene at the start codon was already developed, lentiviral infection and screening for *EPS8L2* knockout clones was performed as before. Here, 60 clones were selected for the screening to increase the chances of identifying a knockout clone. Upon amplification of the target sequence and flanking regions, several clones presented bands with higher electrophoretic mobilities, possibly indicating deletions in the amplified region (Figure 4.2A). Furthermore, some DNA bands with lower molecular weight presented point-mutations or deletions in the start codon region (Figure 4.2B), which could very likely disrupt the expression of Eps8L2. Although, further validation is needed to evaluate the strength of each possible knockout (for example, assessment of mRNA levels through qPCR).

To test whether these mutations in the Eps8L2 coding sequence would have an impact in the nuclear rearward movement phenotype, wound-healing assays were performed. Quantification of the nucleus and centrosome positioning suggested an impaired nuclear movement for clones 1, 3 and 7, presenting values proximal to the non-stimulated control (Figure 4.2C). Furthermore, the percentage of cells reoriented also displayed a decrease in the previous clones, with around 50% of cells presenting their centrosome between the leading edge and the nucleus (Figure 4.2D). Altogether, these results suggest that the deletions previously observed in Eps8L2 DNA sequence from clones 1, 3 and 7, possibly affect the expression of Eps8L2, leading to an impaired nuclear rearward movement. However, nucleus and centrosome positioning as well as centrosome reorientation analyses were performed using only one or two experiments (n=1 or 2). Thus, these results should be validated with more experiments to become reproducible and statistically significant. Moreover, other clones presenting electrophoretic mobilities differences in Figure 4.2A are currently being analysed regarding their nuclear movement phenotype.

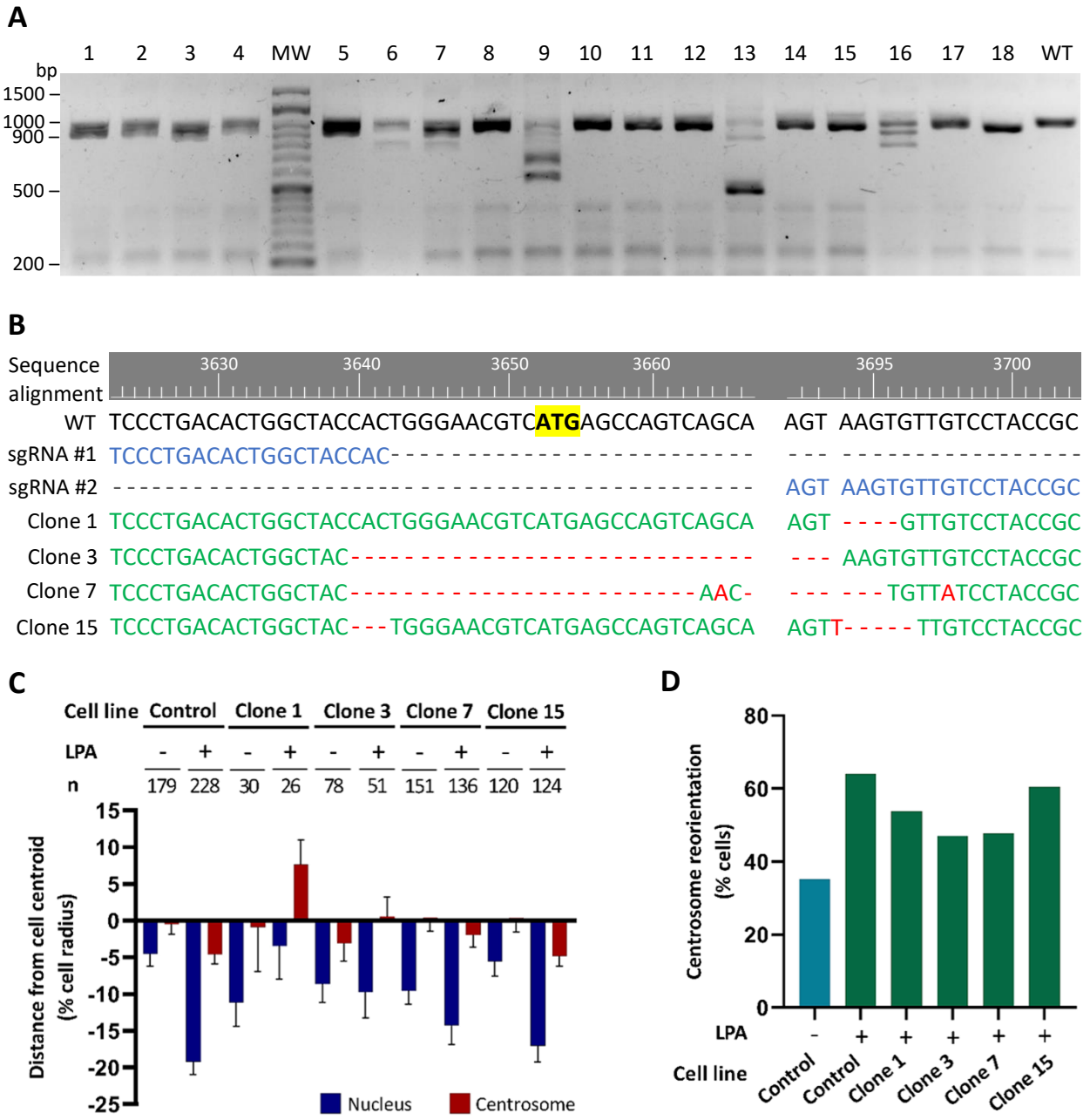

Figure 4.2 Screening for Eps8L2 knockout clones. (A) Agarose electrophoresis for 18 representative Eps8L2 clones (each identified with a number). As a reference, WT (non-transduced) cells, were used. In all cases, an amplicon of approximately 1000 bp is expected for a non-mutated sequence. MW: molecular weight marker. **(B)** Alignment between genomic DNA sequences for clones 1, 3, 7 or 15 and the WT sequence. Two gRNAs were used simultaneously to target the start codon region to increase the likelihood of the desired edit to be performed. The position of each nucleotide indicated was determined using the NCBI reference sequence NC_000073.6. gRNAs used are marked as blue, matching regions as green and mismatching regions as red. The start (ATG) codon is highlighted in yellow in the respective WT sequence. **(C)** Wound-healing assays were performed with clones 1, 3, 7 and 15. WT, non-transduced, cells were used as a Control. Confluent monolayers were starved, wounded and nuclear movement was stimulated with LPA. The average position of the nucleus (blue) and centrosome (red) relative to their distance to the cell centroid (axis origin) were determined. n represents the number of cells quantified. **(D)** Percentage of cells with centrosome reorientation in C. Average ± SEM from two experiments (for Control, clone 7 and clone 15) or one experiment (for clones 1 and 3) is represented.

As an alternative to the endogenous protein tagging, cell lines stably expressing plasmids coding for Myc-Eps8L2, Ctdnep1-GFP (WT protein) or Ctdnep1_D67E-GFP (phosphatase inactive mutant[74]) were generated. Cells expressing the inserted plasmid were selected by drug-selective medium followed by two rounds of FACS selection for GFP-positive cells, thus ensuring that the expression of the tagged-protein was stable.

In the cell lines generated, Ctdnep1 was enriched at the NE and ER, with or without its phosphatase activity (Figure 4.3A). This is consistent with overexpression patterns obtained upon microinjection of cDNA coding for Ctdnep1-GFP or Ctdnep1_D67E-GFP, previously performed in the lab (Supplementary Figure 7.1). Regarding Eps8L2, a homogenous distribution in the cytoplasm and an increased expression inside the nucleus were observed. This expression was not consistent with the overexpression pattern obtained upon microinjection of cDNA coding for Myc-Eps8L2, where the protein was localized in the cytoplasm and enriched near the nucleus, in actin filaments, cell protrusions and the leading edge (Supplementary Figure 7.1).

To check if the nuclear rearward movement phenotype was maintained by the transfected cells, wound-healing assays were performed. Quantification of nucleus and centrosome positioning showed no significant differences between transfected cells and WT non-transfected cells (Control), with the nucleus assuming a positioning proximal to -20% relative to the cell centroid, upon LPA stimulation (Figure 4.3B). Furthermore, the percentage of cells reoriented also displayed no significant differences, with around 65% of stimulated transfected cells (in each condition) presenting centrosome reorientation (Figure 4.3C). Overall, this shows that the stable expression of Ctdnep1-, Ctdnep1_D67E- or Eps8L2-GFP did not affect the nuclear rearward movement.

Both in Ctdnep1 and Eps8L2 cell lines, some cells presented very low expression of GFP tagged proteins, possibly indicating that these cells lose the construct expression over time, which reflects the heterogeneity in the transfect cell population. To transpose this obstacle, a homogenous population of cells can be obtained by serial dilution cloning before the FACS selection for GFP-positive cells[105]. Although this approach would require a longer timeframe to establish a stable expression of the constructs, it would ensure that the stable cell lines were more homogenous after selection, thus possibly expressing the constructs more stably. In parallel, transfection with linear DNA combined with more rounds of FACS selection for GFP-positive cells or lentiviral transduction could be tested, since these have been reported to have higher integration rates in the genome of the cell than circular DNA transfection[106]. These last suggestions are particularly important for Eps8L2-GFP stable cell line, considering the differing overexpression patterns observed.

Given the restricted localization of Ctdnep1 to the NE and ER, both in proximity to the nucleus, this should be the region where Ctdnep1 and Eps8L2 interact. However, since for Eps8L2-GFP, the expression obtained is not concordant with previous expression patterns observed in the lab, further characterization of this cell line is required and even the repetition of the transfection with the above suggested changes.

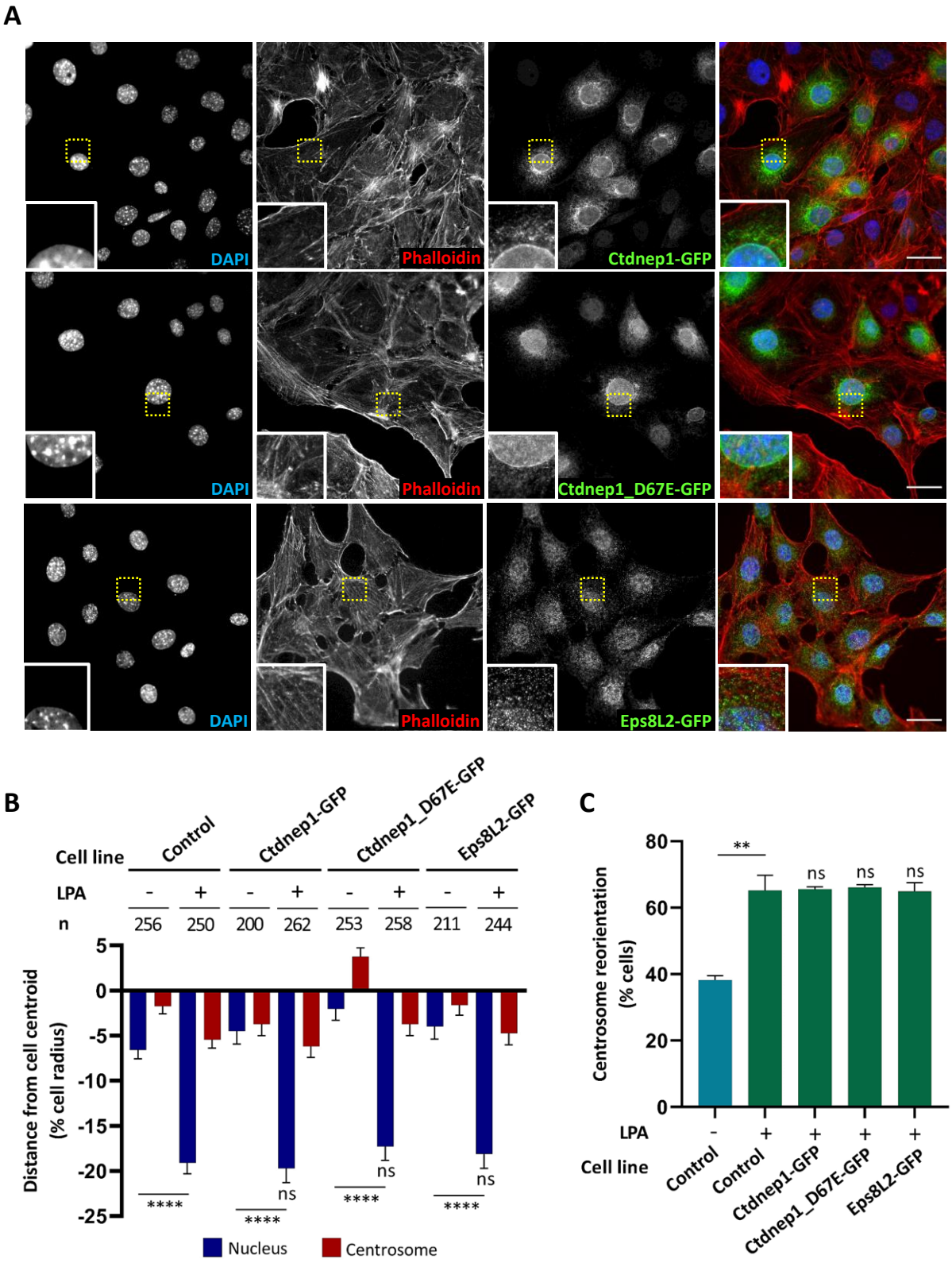

Figure 4.3 Characterization of NIH 3T3 cells stably expressing Ctdnep1-GFP, Ctdnep1_D67E-GFP or Eps8L2-GFP constructs. (A) Representative images of the transfected fibroblasts after the second FACS selection for GFP-positive cells. Staining was performed for DAPI (DNA) shown in blue, phalloidin (F-actin) in red and GFP (Ctdnep1, Ctdnep1_D67E and Eps8L2) in green. The last image of each row results from the merging of all channels. The insets show enlarged views of the yellow regions. Scale bar: 33 µm. **(B)** Wound-healing assays were performed with transfected cells from A. WT, non-transfected, cells were used as a Control. Confluent monolayers were starved, wounded and nuclear movement was stimulated with LPA. The average position of the nucleus (blue) and centrosome (red) relative to their distance to the cell centroid (axis origin) were determined. n represents the number of cells quantified. **(C)** Percentage of cells with centrosome reorientation in B. Average ± SEM from at least three independent experiments is represented. **** P<0,0001; ** P<0,01; ns, P>0,05.

4.2. Eps8L2 dephosphorylation by Ctdnep1

To gain insight into the mechanism through which Ctdnep1 and Eps8L2 physically and directly interact, it was hypothesised that Ctdnep1 could be regulating Eps8L2 actin dynamics through dephosphorylation (Figure 4.4). Upon dephosphorylation, Eps8L2 bundling activity would be stimulated, leading to the formation of actin bundles wide enough to connect to the LINC complex, forming TAN lines and thus resulting in the positioning of the nucleus to the cell rear. In Ctdnep1 or Eps8L2 depleted cells, the LINC complex would be less stably connected or would not properly connect to actin. Consequently, actin-driven forces would be less efficiently transmitted to the nucleus, leading to the previously observed impairment in nuclear rearward movement (section 1.3.3).

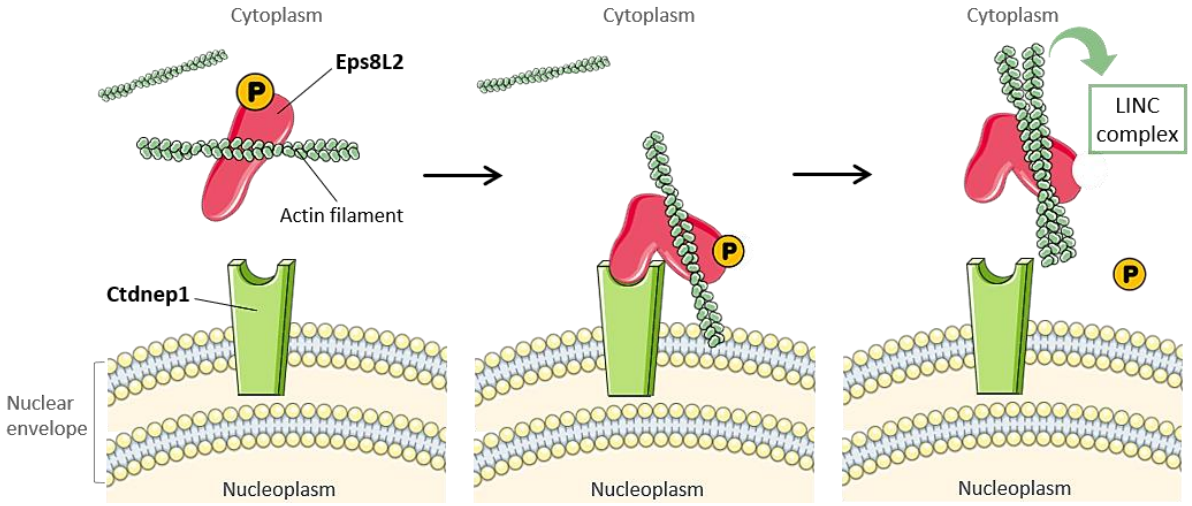

Figure 4.4 Proposed model of Eps8L2 regulation through dephosphorylation by Ctdnep1. At the NE, Ctdnep1 interacts with Eps8L2, which is bound to actin. This interaction is possibly mediated by dephosphorylation and stimulate Eps8L2 bundling activity, leading to the formation of actin bundles wide enough to allow for the coupling of the nucleus to the cytoskeleton through the LINC complex, resulting in nuclear rearward movement.

In fact, this is not the first time that the activation of the Eps8 family of proteins has been associated with protein-protein interactions. It has been described that Eps8 family of proteins is auto-inhibited in vitro and that the interaction with the protein scaffold Abi1 relieves this auto-inhibition and elicits its barbed-end capping activity, leading to the formation of F-actin rich structures[83]. The Eps8-Abi1 complex is also involved in Rac activation, which ultimately leads to actin remodelling[81]. These events do not rule out that additional mechanisms might be in order to optimize the activation of Eps8L2, with dephosphorylation being one of them.

Several phosphoresidues have already been described for Eps8L2, through mass spectrometry in large scale proteomics analyses. These phosphoresidues are: S240, T303, S449, T469 and S570[107–112]. A mechanism of regulation through phosphorylation/dephosphorylation has also been described for Eps8. Its actin barbed-end capping activity is inhibited by phosphorylation of S624 and T628 residues in axonal filopodia formation[113].

Overall these previous studies indicate that Eps8L2 activity can be regulated through protein-protein interactions and, due to the function similarity between different Eps8 family of proteins, this regulation may be stablished through dephosphorylation.

To test the possibility of Eps8L2 being a substrate for Ctdnep1 dephosphorylation, U2OS cells were co-transfected with plasmids coding for Myc-Eps8L2 and Ctdnep1-GFP or Ctdnep1_D67E-GFP. Western blot analysis was conducted to check for any differences in Myc-Eps8L2 molecular weight across the different conditions, which could indicate dephosphorylation. Although, no differences were observed

in Eps8L2 electrophoretic mobility in the presence of Ctdnep1 with or without its phosphatase activity (Figure 4.5A).

To obtain a more sensitive analysis, mass spectrometry of immunoprecipitated Myc-Eps8L2 was conducted to identify phosphorylation sites in Eps8L2 and check for dephosphorylation differences between conditions. Several phosphoresidues were identified, some of which corresponded to the previously reported sites. Although, there were no significant differences in the phosphorylation signal between Eps8L2 in the presence of Ctdnep1 or the phosphatase-dead variant Ctdnep1_D67E (Figure 4.5B).

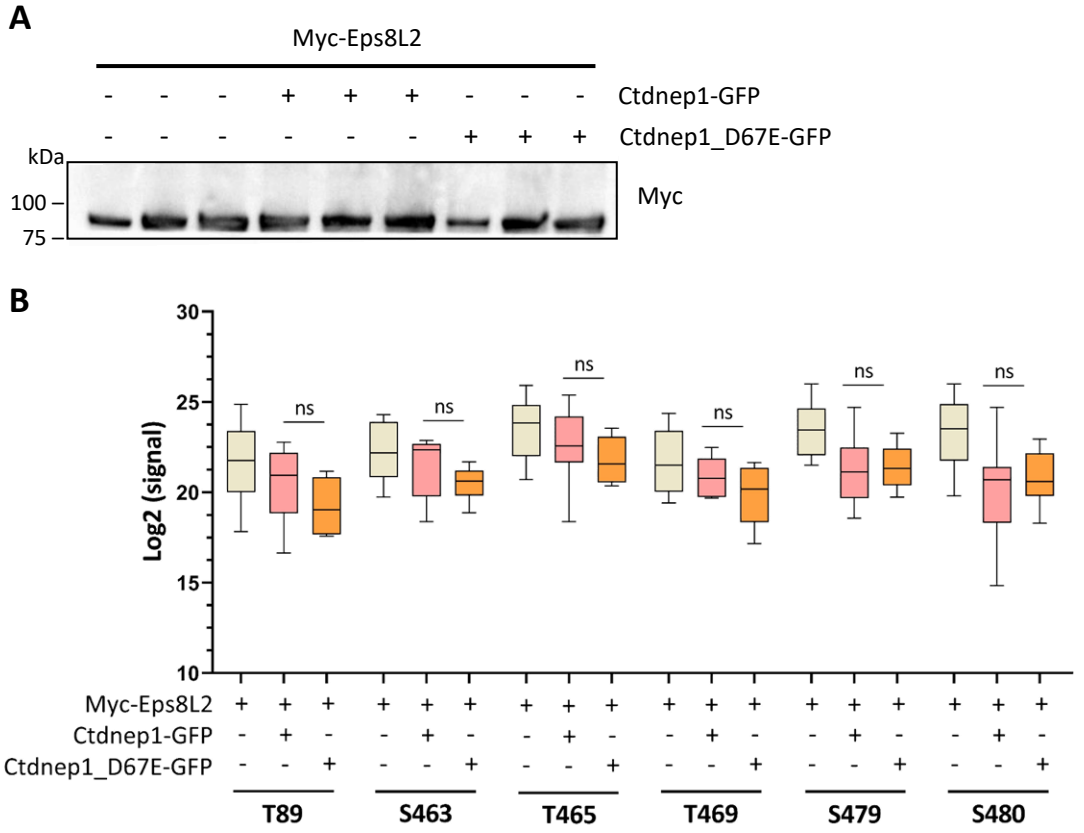

Figure 4.5 Eps8L2 dephosphorylation state in the presence of Ctdnep1 or Ctdnep1_D67E. (A) Western blot analysis for Myc with total cell lysates from U2OS cells co-transfected with plasmids coding for Myc-Eps8L2 and Ctdnep1-GFP or Ctdnep_D67E-GFP. Myc-Eps8L2 has an expected molecular weight of approximately 90 kDa. **(B)** Phosphoresidues identification and respective Log2 (signal) from the mass spectrometry analysis in immunoprecipitated Myc-Eps8L2 from samples in A. Error bars represent SEM from three independent experiments. ns, P>0,05. S: serine; T: threonine.

It has been reported that Ctdnep1 is only able to dephosphorylate another downstream target, Lipin, in the presence of a regulatory subunit termed Nep1-r1. Han and colleagues showed that in the simultaneous presence of Ctdnep1 and Nep1-r1, Lipin-1 or -2 presented an increased electrophoretic mobility that correlated with Lipin dephosphorylation (Supplementary Figure 7.2)[76]. To check if this was the case for Myc-Eps8L2 possible dephosphorylation, U2OS cells were co-transfected with Myc-Eps8L2, Nep1-r1-HA-ProtA and Ctdnep1-GFP or Ctdnep1_D67E-GFP. Co-transfection with Lipin-2-V5 instead of Myc-Eps8L2 was performed as a control for the experimental approach.

Through Western blot analysis, there were no electrophoretic mobility differences in Lipin-2 in the presence of Ctdnep1 and Nep1-r1 (Figure 4.6A), contrary to what was reported. Regarding Eps8L2, besides not detecting electrophoretic mobility differences in the presence of Ctdnep1 and Nep1-r1, a decrease in molecular weight with lambda (λ) phosphatase treatment (total dephosphorylation) was also not observed (Figure 4.6B). The lack of mobility shift in the lambda phosphatase control could be

explained by the sensitivity of the Western blot approach. In one hand, Lipin-2 has at least 21 phosphoresidues identified[114] and the molecular weight difference from the phosphorylated protein and the dephosphorylated counterpart is within the range of discrimination of the gel and reported[76]. For Eps8L2, the total number of phosphoresidues and the total dephosphorylation shift are unknown and thus may fall out of the sensitivity range of the gel. On the other hand, to increase the sensitivity of the dephosphorylation shift analysis, Phos-tag gels could be used. These incorporate a phosphate capture molecule, which binds to and delays migration of phosphorylated proteins. Thus, an increased shift in the electrophoretic mobility of phosphorylated proteins is observed, in comparison to their dephosphorylated counterpart[115].

Although it was not possible to observe significant differences in Eps8L2 electrophoretic mobility in the presence of Nep1-r1 and Ctdnep1 or Ctdnep1_D67E, mass spectrometry of purified Myc-Eps8L2 was used to obtain a more sensitive analysis regarding the phosphorylation state of Eps8L2. Several phosphosites were identified, most of which were coincident with the previous analysis. Again, there were no significant differences in the phosphorylation signal between different conditions (Figure 4.6C). Although, it was noted that replicate 1 of lysates with Ctdnep1_D67E had a lower amount of protein than replicates 2 and 3 (data not shown). Additionally, when removing this replicate from the quantification in Figure 4.6C, no significant differences between conditions were observed in the majority of the identified phosphosites, except for S479 and S480 (Figure 4.6D). These residues now presented a significant signal reduction in the presence of Ctdnep1, in comparison to Ctdnep1_D67E lysates, suggesting that Ctdnep1 was dephosphorylating S479 and S480. Further analysis is required to confirm the dephosphorylation of S479 and S480 by Ctdnep1. Currently, NIH 3T3 cells are being microinjected with cDNA coding for phosphomutant variants of Eps8L2, one that mimics phosphorylation (S479DS480D) and another one that mimics dephosphorylation (S479AS480A), to test if there is a rescue of nuclear rearward movement in fibroblasts treated with Ctdnep1 siRNA.

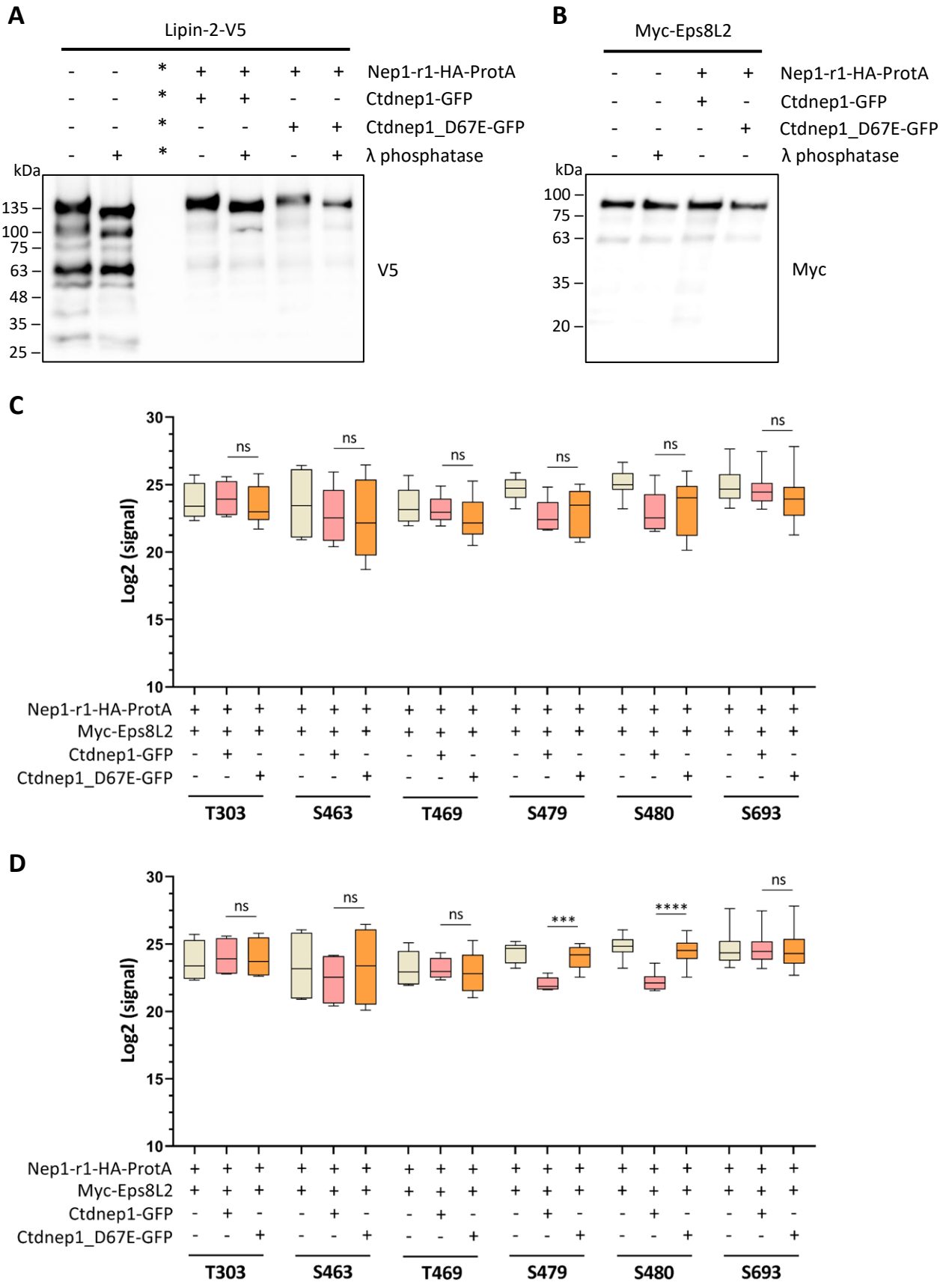

Figure 4.6 Eps8L2 and Lipin dephosphorylation state in the presence of Nep1-r1 and Ctdnep1 or Ctdnep1_D67E. (A,B) Western blot analysis for V5 or Myc, respectively, with total cell lysates from U2OS cells co-transfected with plasmids coding for Lipin-2-V5 or Myc-Eps8L2 in the presence of Nep1-r1-HA-ProtA and Ctdnep1-GFP or Ctdnep_D67E-GFP. Lambda (λ) phosphatase treatment was used as a control for total dephosphorylation of Lipin-2 and Eps8L2. Lipin-2-V5 has an expected

molecular weight of approximately 130 kDa, while Myc-Eps8L2 has approximately 90 kDa. The asterisk denotes the lane with the molecular weight marker. **(C)** Phosphoresidues identification and respective Log_2 (signal) from the mass spectrometry analysis in immunoprecipitated Myc-Eps8L2 from B. **(D)** Log_2 (signal) of phosphoresidues from C without replicate 1. Error bars represent SEM from three (C) or two (D) independent experiments. **** P<0,0001; *** P<0,001; ns, P>0,05. S: serine; T: threonine.

4.3. Ctdnep1 and Eps8L2 role in cell migration

Nuclear positioning plays a crucial role in proper cell migration. Considering that Ctdnep1 and Eps8L2 knockdowns were shown to impair nuclear movement, the possibility that these would also impair cell migration in a 2D substrate was tested. Wound-healing assays were performed and wound closure area over a course of 16 h in Control, Ctdnep1 or Eps8L2 siRNAs monolayers was quantified (Figure 4.7A). No significant differences were observed in wound closure area capability between the different conditions (Figure 4.7B and C). Therefore, these results do not support an involvement of Ctdnep1 and Eps8L2 in 2D cell migration in the present experimental conditions. Although, this does not completely exclude a potential role for Ctdnep1 and Eps8L2 during 2D migration, since the impact of this interaction in the velocity and persistence of 2D random migration should also be analysed. Furthermore, there is the potential for Ctdnep1 and Eps8L2 to be important during migration in 3D matrixes.

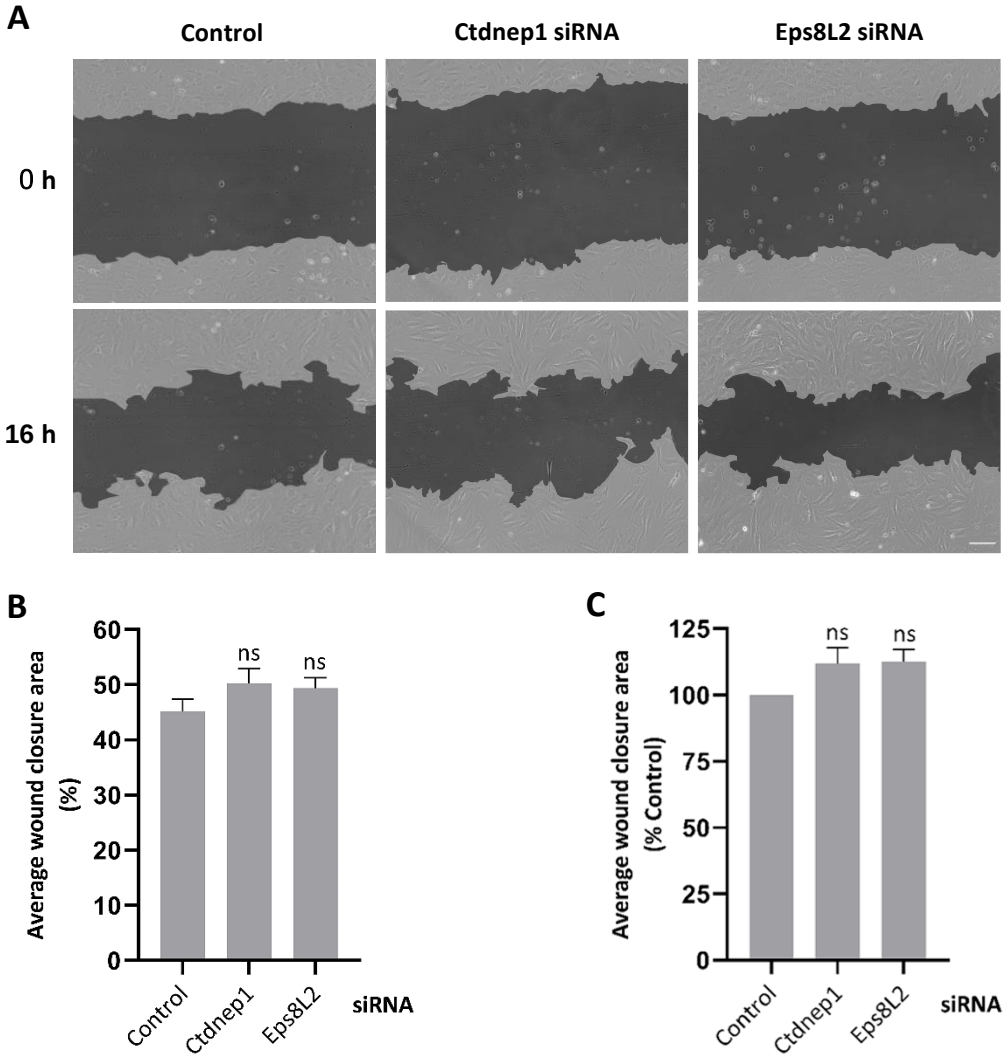

Figure 4.7 Ctdnep1 and Eps8L2 in cell migration. NIH 3T3 cells were treated with Control, Ctdnep1 or Eps8L2 siRNAs and wound-healing assays were performed. Confluent monolayers were starved, wounded and cell migration was stimulated with complete culture medium. **(A)** Representative images of the wound closure area at 0 h and 16 h of acquisition. Scale bar:

108 μm. **(B, C)** Quantification of the average wound closure area (in % or relative to Control, respectively), 16 h after wound. Average ± SEM from three independent experiments is represented. ns, P>0,05.

There are substantial differences between 2D and 3D cell migration, which is reflected on nuclear dynamics. In 3D substrates, cells not only feel external cues and move around surfaces, but also squeeze, reshape and manipulate the surrounding environment[116]. Consequently, ECM properties (such as stiffness, matrix pore size, confinement and crosslinking) can impose unique constraints on cell motility not present in liquid media[117]. This leads to different morphologies and migration modes. In 2D substrates, fibroblasts use actin polymerization to extend the leading edge in a lamellipodia-based migration. In 3D substrates, these cells can alternate between a low-pressure lamellipodia-, high-pressure lobopodia- and amoeboid fibroblast-based migration, in response to the physical properties of the extracellular matrix[117,118].

Fibroblasts' morphology plasticity entails nuclear deformation and movement (to the back or front depending on the migration mode) through molecular pathways essential for 3D motility, yet not required by cells in a rigid 2D surface [29,119,120]. Thus, there is the possibility that despite Ctdnep1 and Eps8L2 absence did not impair 2D wound-closure capability in cell migration, it can be important in 3D matrixes. At the molecular level, it is known that a greater nuclear and cytoskeletal deformation is required to pass through narrow spaces in 3D substrates. Thus, the coupling between the nucleus and the cytoskeleton would affect cell migration. This could be provided by Eps8L2 bundling activity, which is hypothesized to be activated by Ctdnep1 and crucial for connecting actin bundles to the LINC complex.

Several 3D systems can be used to mimic the narrow interstitial spaces of the tissue environment. From these, microfluidic devices allow a tighter control over the device morphology. The devices consist of a cross-linked polymer (usually PDMS) into a microstructured mold, creating channels of defined geometries through which cells must migrate[121]. Microfluidic devices have been widely applied to study cancer cell migration[26], including at single-cell resolution that provides retrieval of distinct migrating cell populations for further characterization[122,123]. Thus, besides mimicking the ECM, these devices also provide resources to further dissect the molecular differences between an heterogeneous migrating cell population, therefore presenting a great potential to investigate the role of Ctdnep1 and Eps8L2 in 3D cell migration.

5. Conclusions and future perspectives

This work provides further evidence for the role of Ctdnep1-Eps8L2 interaction in actin organization as well as its implications during nuclear positioning in migrating fibroblasts. It is demonstrated that Ctdnep1 localizes to the NE and ER (independently of its phosphatase activity), while Eps8L2 was distributed along the cytoplasm. Since Ctdnep1 localization is restricted to the NE and ER, especially near the nucleus, this should be the region where Ctdnep1 and Eps8L2 interact. Regarding the mechanism underlying this interaction, S479 and S480 were identified as two possible substrates for Eps8L2 dephosphorylation by Ctdnep1, supporting the proposed model for the physical and direct interaction between the two proteins. Furthermore, when inquiring about the extent of Ctdnep1 and Eps8L2 role in cell migration, no significant differences were observed in the wound closure capability of 2D-migrating fibroblasts.

Future work should focus on exploring each of these subjects (subcellular localization, mechanism of interaction and role in cell migration) in more detail to answer pending questions: Does Ctdnep1 and Eps8L2 subcellular localization changes throughout migration and does this localization affect one another? This question could now be answered using the stable cell line system developed in the present work in combination with targeted siRNA treatment or using the knockout cell lines currently being generated. Does Eps8L2 localizes to TAN lines and, if so, is this localization dependent on the dephosphorylation of the two identified serines? Moreover, is Eps8L2 actin bundling activity regulated by these dephosphorylation events? Answering these questions is crucial to validate the proposed model for the mechanism of interaction between Ctdnep1 and Eps8L2. And what about 3D cell migration? Studying the molecular mechanisms of nuclear movement in 3D environments, rather than on 2D tissue culture plastic, will afford a greater complexity and thus is likely to provide the most efficient way to address the role of Ctdnep1 and Eps8L2 during migration. To further characterize Ctdnep1-Eps8L2 interaction, other details should also be explored, such as the possible role of the interaction in mechanotransduction and gene expression or its coordination with other previously reported mechanisms for regulating LINC complex and TAN lines dynamics.

Ultimately, this study sheds light on the importance of identifying new players in the complex and refined network that regulates nuclear positioning. Deciphering the mechanisms connecting the nucleus to the cytoskeleton is valuable to better understand important physiological correlations between nuclear positioning and disease.

6. References

1. Alberts, B. *et al. Molecular biology of the cell*. (Garland Science, 2015).
2. Wilson, K. L. & Dawson, S. C. Functional evolution of nuclear structure. *J. Cell Biol.* **195**, 171–81 (2011).
3. Gruenbaum, Y. & Foisner, R. Lamins: nuclear intermediate filament proteins with fundamental functions in nuclear mechanics and genome regulation. *Annu. Rev. Biochem.* **84**, 131–64 (2015).
4. de Leeuw, R., Gruenbaum, Y. & Medalia, O. Nuclear lamins: thin filaments with major functions. *Trends Cell Biol.* **28**, 34–45 (2018).
5. Maniotis, A. J., Chen, C. S. & Ingber, D. E. Demonstration of mechanical connections between integrins, cytoskeletal filaments, and nucleoplasm that stabilize nuclear structure. *Proc. Natl. Acad. Sci.* **94**, 849–54 (1997).
6. Padmakumar, V. C. *et al.* The inner nuclear membrane protein Sun1 mediates the anchorage of Nesprin-2 to the nuclear envelope. *J. Cell Sci.* **118**, 3419–30 (2005).
7. Münter, S. *et al.* Actin polymerisation at the cytoplasmic face of eukaryotic nuclei. *BMC Cell Biol.* **7**, 23 (2006).
8. Preston, C. & Faustino, R. Nuclear envelope regulation of oncogenic pocesses: roles in pancreatic cancer. *Epigenomes* **2**, 15 (2018).
9. Gundersen, G. G. & Worman, H. J. Nuclear positioning. *Cell* **152**, 1376–89 (2013).
10. Baye, L. M. & Link, B. A. Interkinetic nuclear migration and the selection of neurogenic cell divisions during vertebrate retinogenesis. *J. Neurosci.* **27**, 10143–52 (2007).
11. Spear, P. C. & Erickson, C. A. Interkinetic nuclear migration: a mysterious process in search of a function. *Dev. Growth Differ.* **54**, 306–16 (2012).
12. Tomlinson, A. & Ready, D. F. Neuronal differentiation in the Drosophila ommatidium. *Dev. Biol.* **120**, 366–76 (1987).
13. Patterson, K. The functions of Klarsicht and nuclear lamin in developmentally regulated nuclear migrations of photoreceptor cells in the Drosophila eye. *Mol. Biol. Cell* **15**, 600–10 (2003).
14. Cadot, B. *et al.* Nuclear movement during myotube formation is microtubule and dynein dependent and is regulated by Cdc42, Par6 and Par3. *EMBO Rep.* **13**, 741–9 (2012).
15. Roman, W. & Gomes, E. R. Nuclear positioning in skeletal muscle. *Semin. Cell Dev. Biol.* **82**, 51–56 (2018).
16. Moore, J. K., Stuchell-Brereton, M. D. & Cooper, J. A. Function of dynein in budding yeast: Mitotic spindle positioning in a polarized cell. *Cell Motil. Cytoskeleton* **66**, 546–55 (2009).
17. Tran, P. T., Marsh, L., Doye, V., Inoué, S. & Chang, F. A mechanism for nuclear positioning in fission yeast based on microtubule pushing. *J. Cell Biol.* **153**, 397–412 (2001).
18. Gilbert, S. F. *Developmental Biology*. (Sinauer Associates Inc., 2016).
19. Davidson, P. M., Denais, C., Bakshi, M. C. & Lammerding, J. Nuclear deformability constitutes a rate-limiting step during cell migration in 3-D environments. *Cell. Mol. Bioeng.* **7**, 293–306 (2014).
20. Calero-Cuenca, F. J., Janota, C. S. & Gomes, E. R. Dealing with the nucleus during cell migration. *Curr. Opin. Cell Biol.* **50**, 35–41 (2018).
21. Barzilai, S. *et al.* Leukocytes breach endothelial barriers by insertion of nuclear lobes and disassembly of endothelial actin filaments. *Cell Rep.* **18**, 685–99 (2017).
22. Fu, Y., Chin, L. K., Bourouina, T., Liu, A. Q. & Vandongen, A. M. J. Nuclear deformation during breast cancer cell transmigration. *Lab Chip* **12**, 3774–8 (2012).
23. Harada, T. *et al.* Nuclear lamin stiffness is a barrier to 3D migration, but softness can limit survival. *J. Cell Biol.* **204**, 669–82 (2014).
24. Thomas, D. G. *et al.* Non-muscle myosin IIB is critical for nuclear translocation during 3D invasion. *J. Cell Biol.* **210**, 583–94 (2015).

25. Navarro-Lérida, I. *et al.* Rac1 nucleocytoplasmic shuttling drives nuclear shape changes and tumor invasion. *Dev. Cell* **32**, 318–34 (2015).

26. Denais, C. M. *et al.* Nuclear envelope rupture and repair during cancer cell migration. *Science* **352**, 353–58 (2016).

27. Raab, M. *et al.* ESCRT III repairs nuclear envelope ruptures during cell migration to limit DNA damage and cell death. *Science* **352**, 359–62 (2016).

28. Manley, H. R., Keightley, M. C. & Lieschke, G. J. The neutrophil nucleus: an important influence on neutrophil migration and function. *Front. Immunol.* **9**, 2867 (2018).

29. Doyle, A. D., Petrie, R. J., Kutys, M. L. & Yamada, K. M. Dimensions in cell migration. *Curr. Opin. Cell Biol.* **25**, 642–49 (2013).

30. Petrie, R. J. & Yamada, K. M. Fibroblasts Lead the Way: A Unified View of 3D Cell Motility. *Trends Cell Biol.* **25**, 666–74 (2015).

31. Bone, C. R. & Starr, D. A. Nuclear migration events throughout development. *J. Cell Sci.* **129**, 1951–61 (2016).

32. Lee, Y. L. & Burke, B. LINC complexes and nuclear positioning. *Semin. Cell Dev. Biol.* **82**, 67–76 (2018).

33. Gomes, E. R. & Jani, S. Nuclear Movement Regulated by Cdc42, MRCK, Myosin, and Actin Flow Establishes MTOC Polarization in Migrating Cells. *Cell* **121**, 451–63 (2005).

34. Gomes, E. R. & Gundersen, G. G. Real-time centrosome reorientation during fibroblast migration. *Methods Enzymol.* **406**, 579–92 (2006).

35. Tsai, L. H. & Gleeson, J. G. Nucleokinesis in neuronal migration. *Neuron* **46**, 383–8 (2005).

36. Barnhart, E. L., Allen, G. M., Jülicher, F. & Theriot, J. A. Bipedal locomotion in crawling cells. *Biophys. J.* **98**, 933–42 (2010).

37. Dornier, E. & Norman, J. C. Cancer cells with trapped nuclei cut their way through the extracellular matrix. *Nat. Commun.* **9**, 3954 (2018).

38. Luxton, G. W. G., Gomes, E. R., Folker, E. S., Vintinner, E. & Gundersen, G. G. Linear arrays of nuclear envelope proteins harness retrograde actin flow for nuclear movement. *Science* **329**, 956–9 (2010).

39. Cain, N. E. *et al.* Conserved SUN-KASH interfaces mediate LINC complex-dependent nuclear movement and positioning. *Curr. Biol.* **28**, 3086–97 (2018).

40. Starr, D. A. & Han, M. Role of ANC-1 in tethering nuclei to the actin cytoskeleton. *Science* **298**, 406–9 (2002).

41. Lee, K., Starr D., Cohen M., Liu J., Han M., Wilson KL., G. Y. Lamin-dependent localization of UNC-84, a protein required for nuclear migration in Caenorhabditis elegans. *Mol. Biol. Cell* **13**, 892–901 (2002).

42. Sosa, B. A., Rothballer, A., Kutay, U. & Schwartz, T. U. LINC complexes form by binding of three KASH peptides to domain interfaces of trimeric SUN proteins. *Cell* **149**, 1035–47 (2012).

43. Hao, H. & Starr, D. A. SUN/KASH interactions facilitate force transmission across the nuclear envelope. *Nucleus* **10**, 73–80 (2019).

44. Lele, T. P., Dickinson, R. B. & Gundersen, G. G. Mechanical principles of nuclear shaping and positioning. *J. Cell Biol* **217**, 3330–42 (2018).

45. Neelam, S. *et al.* Direct force probe reveals the mechanics of nuclear homeostasis in the mammalian cell. *Proc. Natl. Acad. Sci. U. S. A.* **112**, 5720–5 (2015).

46. Arsenovic, P. T. *et al.* Nesprin-2G, a component of the nuclear LINC complex, is subject to myosin-dependent tension. *Biophys. J.* **110**, 34–43 (2016).

47. Zhu, R., Antoku, S. & Gundersen, G. G. Centrifugal displacement of nuclei reveals multiple LINC complex mechanisms for homeostatic nuclear positioning. *Curr. Biol.* **27**, 3097–3110 (2017).

48. Alam, S. G. *et al.* The nucleus is an intracellular propagator of tensile forces in NIH 3T3 fibroblasts. *J. Cell Sci.* **128**, 1901–11 (2015).

49. Almonacid, M., Terret, M. E. & Verlhac, M. H. Nuclear positioning as an integrator of cell fate. *Current Opinion in Cell Biology* **56**, 122–29 (2019).

50. Dominguez, R. & Holmes, K. C. Actin structure and function. *Annu. Rev. Biophys.* **40**, 169–86 (2011).

51. Gant Luxton, G. W., Gomes, E. R., Folker, E. S., Worman, H. J. & Gundersen, G. G. TAN lines: A novel nuclear envelope structure involved in nuclear positioning. *Nucleus* **2**, 173–81 (2011).

52. Borrego-Pinto, J. *et al.* Samp1 is a component of TAN lines and is required for nuclear movement. *J. Cell Sci.* **125**, 1099–1105 (2012).

53. Saunders, C. A. *et al.* TorsinA controls TAN line assembly and the retrograde flow of dorsal perinuclear actin cables during rearward nuclear movement. *J. Cell Biol.* **216**, 657–74 (2017).

54. Kutscheidt, S. *et al.* FHOD1 interaction with nesprin-2G mediates TAN line formation and nuclear movement. *Nat. Cell Biol.* **16**, 708–15 (2014).

55. Jayo, A. *et al.* Fascin regulates nuclear movement and deformation in migrating cells. *Dev. Cell* **38**, 371–83 (2016).

56. Dobrzynska, A., Gonzalo, S., Shanahan, C. & Askjaer, P. The nuclear lamina in health and disease. *Nucleus* **7**, 233–48 (2016).

57. Kang, S. mi, Yoon, M. H. & Park, B. J. Laminopathies; Mutations on single gene and various human genetic diseases. *BMB Rep.* **51**, 327–337 (2018).

58. Crasto, S. & Di Pasquale, E. Induced pluripotent stem cells to study mechanisms of laminopathies: focus on epigenetics. *Front. Cell Dev. Biol.* **6**, 172 (2018).

59. Janin, A. & Gache, V. Nesprins and lamins in health and diseases of cardiac and skeletal muscles. *Front. Physiol.* **9**, 1277 (2018).

60. Folker, E. S., Östlund, C., Luxton, G. W. G., Worman, H. J. & Gundersen, G. G. Lamin A variants that cause striated muscle disease are defective in anchoring transmembrane actin-associated nuclear lines for nuclear movement. *Proc. Natl. Acad. Sci. U. S. A.* **108**, 131–6 (2011).

61. Sakthivel, K. M. & Sehgal, P. A novel role of lamins from genetic disease to cancer biomarkers. *Oncol. Rev.* **10**, 309 (2016).

62. Matsumoto, A. *et al.* Global loss of a nuclear lamina component, lamin A/C, and LINC complex components SUN1, SUN2, and nesprin-2 in breast cancer. *Cancer Med.* **4**, 1547–57 (2015).

63. Guinde, J. *et al.* Lamins in lung cancer: biomarkers and key factors for disease progression through miR-9 regulation? *Cells* **7**, 78 (2018).

64. Saarinen, I., Mirtti, T., Seikkula, H., Boström, P. J. & Taimen, P. Differential predictive roles of A-and B-type nuclear lamins in prostate cancer progression. *PLoS One* **10**, e0140671 (2015).

65. Winter, L. & Wiche, G. The many faces of plectin and plectinopathies: pathology and mechanisms. *Acta Neuropathol.* **125**, 77–93 (2013).

66. Clemen, C. S., Herrmann, H., Strelkov, S. V & Schröder, R. Desminopathies: pathology and mechanisms. *Acta Neuropathol.* **125**, 47–75 (2013).

67. Tasfaout, H., Cowling, B. S. & Laporte, J. Centronuclear myopathies under attack: A plethora of therapeutic targets. *J. Neuromuscul. Dis.* **5**, 387–406 (2018).

68. Meinke, P. *et al.* Muscular dystrophy-associated SUN1 and SUN2 variants disrupt nuclear-cytoskeletal connections and myonuclear organization. *PLoS Genet.* **10**, e1004605 (2014).

69. Calvi, A. *et al.* SUN4 is essential for nuclear remodeling during mammalian spermiogenesis. *Dev. Biol.* **407**, 321–30 (2015).

70. Haithcock, E. *et al.* Age-related changes of nuclear architecture in Caenorhabditis elegans. *Proc. Natl. Acad. Sci.* **102**, 16690–5 (2005).

71. Chang, W. *et al.* Imbalanced nucleocytoskeletal connections create common polarity defects in progeria and physiological aging. *Proc. Natl. Acad. Sci.* **116**, 3578–83 (2019).

72. Satow, R., Chan, T. C. & Asashima, M. Molecular cloning and characterization of dullard: a novel gene required for neural development. *Biochem. Biophys. Res. Commun.* **295**, 85–91 (2002).

73. Kim, Y. *et al.* A conserved phosphatase cascade that regulates nuclear membrane biogenesis. *Proc. Natl. Acad. Sci. U. S. A.* **104**, 6596–601 (2007).

74. Satow, R., Kurisaki, A., Chan, T. chuan, Hamazaki, T. S. & Asashima, M. Dullard promotes degradation and dephosphorylation of BMP receptors and is required for neural induction. *Dev. Cell* **11**, 763–74 (2006).

75. Tanaka, S. S., Nakane, A., Yamaguchi, Y. L., Terabayashi, T. & Abe, T. Dullard/Ctdnep1 modulates WNT signalling activity for the formation of primordial germ cells in the mouse embryo. *PLoS One* **8**, e57428 (2013).

76. Han, S. *et al.* Nuclear envelope phosphatase 1-regulatory subunit 1 (Formerly TMEM188) is the metazoan Spo7p ortholog and functions in the lipin activation pathway. *J. Biol. Chem.* **287**, 3123–37 (2012).

77. Bahmanyar, S. *et al.* Spatial control of phospholipid flux restricts endoplasmic reticulum sheet formation to allow nuclear envelope breakdown. *Genes Dev.* **28**, 121–6 (2014).

78. Jones, D. T. W. *et al.* Dissecting the genomic complexity underlying medulloblastoma. *Nature* **488**, 100–5 (2012).

79. Pugh, T. J. *et al.* Medulloblastoma exome sequencing uncovers subtype-specific somatic mutations. *Nature* **488**, 106–10 (2012).

80. Paine, M. R. L. *et al.* Three-dimensional mass spectrometry imaging identifies lipid markers of medulloblastoma metastasis. *Sci. Rep.* **9**, 2205 (2019).

81. Offenhäuser, N. *et al.* The Eps8 family of proteins links growth factor stimulation to actin reorganization generating functional redundancy in the Ras/Rac pathway. *Mol. Biol. Cell* **15**, 91–8 (2004).

82. Hertzog, M. *et al.* Molecular basis for the dual function of Eps8 on actin dynamics: bundling and capping. *PLoS Biol.* **8**, e1000387 (2010).

83. Disanza, A. *et al.* Eps8 controls actin-based motility by capping the barbed ends of actin filaments. *Nat. Cell Biol.* **6**, 1180–8 (2004).

84. Disanza, A. *et al.* Regulation of cell shape by Cdc42 is mediated by the synergic actin-bundling activity of the Eps8-IRSp53 complex. *Nat. Cell Biol.* **8**, 1337–47 (2006).

85. Furness, D. N. *et al.* Progressive hearing loss and gradual deterioration of sensory hair bundles in the ears of mice lacking the actin-binding protein Eps8L2. *Proc. Natl. Acad. Sci. U. S. A.* **110**, 13898–903 (2013).

86. Dunn, J. *et al.* Proteomic analysis discovers the differential expression of novel proteins and phosphoproteins in meningioma including NEK9, HK2 and SET and deregulation of RNA metabolism. *EBioMedicine* **40**, 77–91 (2019).

87. Calero-Cuenca, F. J. *et al.* Ctdnep1 and Eps8L2 regulate dorsal actin cables for nuclear positioning during cell migration. (2019) (under review).

88. Schindelin, J. *et al.* Fiji: An open-source platform for biological-image analysis. *Nature Methods* **9**, 676–82 (2012).

89. Thomas, L. S. V. & Gehrig, J. Multi-Template Matching: a versatile tool for object-localization in microscopy images. *bioRxiv* 619338 (2019).

90. Gundersen, G. G., Kim, I. & Chapin, C. J. Induction of stable microtubules in 3T3 fibroblasts by TGF-beta and serum. *J. Cell Sci.* **107 (Pt 3)**, 645–59 (1994).

91. Cook, T. A., Nagasaki, T. & Gundersen, G. G. Rho guanosine triphosphatase mediates the selective stabilization of microtubules induced by lysophosphatidic acid. *J. Cell Biol.* **141**, 175–85 (1998).

92. Chang, W., Antoku, S. & Gundersen, G. G. Wound-healing assays to study mechanisms of nuclear movement in fibroblasts and myoblasts. *Methods Mol. Biol.* **1411**, 255–67 (2016).

93. Chang, W. Cell Plot software. *Greg Gundersen Lab, Columbia University Medical Center* Available at: http://www.columbia.edu/~wc2383/software.html.

94. Sanjana, N. E., Shalem, O. & Zhang, F. Improved vectors and genome-wide libraries for CRISPR screening. *Nature Methods* **11**, 783–4 (2014).

95. Shalem, O. *et al.* Genome-scale CRISPR-Cas9 knockout screening in human cells. *Science* **343**, 84–7 (2014).

96. Haeussler, M. *et al.* Evaluation of off-target and on-target scoring algorithms and integration into the guide RNA selection tool CRISPOR. *Genome Biol.* **17**, 148 (2016).

97. GSL Biotech. SnapGene sotware. Available at: https://www.snapgene.com/.

98. Hughes, C. S. *et al.* Ultrasensitive proteome analysis using paramagnetic bead technology. *Mol. Syst. Biol.* **10**, 757 (2014).

99. GraphPad software. Available at: https://www.graphpad.com/.

100. Cong, L. & Zhang, F. Genome engineering using CRISPR-Cas9 system. *Methods Mol. Biol.* **1239**, 197–217 (2015).

101. Lin, S., Staahl, B. T., Alla, R. K. & Doudna, J. A. Enhanced homology-directed human genome engineering by controlled timing of CRISPR/Cas9 delivery. *Elife* **3**, e04766 (2014).

102. Chu, V. T. *et al.* Increasing the efficiency of homology-directed repair for CRISPR-Cas9-induced precise gene editing in mammalian cells. *Nat. Biotechnol.* **33**, 543–8 (2015).

103. Charpentier, M. *et al.* CtIP fusion to Cas9 enhances transgene integration by homology-dependent repair. *Nat. Commun.* **9**, 1133 (2018).

104. Savic, N. *et al.* Covalent linkage of the DNA repair template to the CRISPR-Cas9 nuclease enhances homology-directed repair. *Elife* **7**, e33761 (2018).

105. A. Longo, P., Kavran, J. M., Kim, M. S. & Leahy, D. J. Generating mammalian stable cell lines by electroporation. *Methods Enzymol.* **529**, 209–26 (2013).

106. Elegheert, J. *et al.* Lentiviral transduction of mammalian cells for fast, scalable and high-level production of soluble and membrane proteins. *Nat. Protoc.* **13**, 2991–3017 (2018).

107. Villén, J., Beausoleil, S. A., Gerber, S. A. & Gygi, S. P. Large-scale phosphorylation analysis of mouse liver. *Proc. Natl. Acad. Sci. U. S. A.* **104**, 1488–93 (2007).

108. Cantin, G. T. *et al.* Combining protein-based IMAC, peptide-based IMAC, and MudPIT for efficient phosphoproteomic analysis. *J. Proteome Res.* **7**, 1346–51 (2008).

109. Dephoure, N. *et al.* A quantitative atlas of mitotic phosphorylation. *Proc. Natl. Acad. Sci. U. S. A.* **105**, 10762–67 (2008).

110. Huttlin, E. L. *et al.* A tissue-specific atlas of mouse protein phosphorylation and expression. *Cell* **143**, 1174–89 (2010).

111. Zhou, H. *et al.* Toward a comprehensive characterization of a human cancer cell phosphoproteome. *J. Proteome Res.* **12**, 260–71 (2013).

112. Bian, Y. *et al.* An enzyme assisted RP-RPLC approach for in-depth analysis of human liver phosphoproteome. *J. Proteomics* **96**, 253–62 (2014).

113. Menna, E. *et al.* Eps8 regulates axonal filopodia in hippocampal neurons in response to brain-derived neurotrophic factor (BDNF). *PLoS Biol.* **7**, e1000138 (2009).

114. Peterson, T. R. *et al.* mTOR complex 1 regulates lipin 1 localization to control the SREBP pathway. *Cell* **146**, 408–20 (2011).

115. Nagy, Z., Comer, S. & Smolenski, A. Analysis of protein phosphorylation using Phos-tag gels. *Curr. Protoc. protein Sci.* **93**, e64 (2018).

116. Lautscham, L. A. *et al.* Migration in confined 3D environments is determined by a combination of adhesiveness, nuclear volume, contractility, and cell stiffness. *Biophys. J.* **109**, 900–13 (2015).

117. Petrie, R. J. & Yamada, K. M. At the leading edge of three-dimensional cell migration. *J. Cell Sci.* **125**, 5917–26 (2012).

118. Berre, L. *et al.* Confinement and low adhesion induce fast amoeboid migration of slow mesenchymal cells. *Cell* **160**, 659–72 (2015).

119. DeSimone, D. W. & Horwitz, A. R. Many modes of motility. *Science* **345**, 1002–3 (2014).

120. Graham, D. M. *et al.* Enucleated cells reveal differential roles of the nucleus in cell migration, polarity, and mechanotransduction. *J. Cell Biol.* **217**, 895–914 (2018).

121. Keys, J., Windsor, A. & Lammerding, J. Assembly and use of a microfluidic device to study cell migration in confined environments. *Methods Mol. Biol.* **1840**, 101–18 (2018).

122. Chen, Y. C. *et al.* Single-cell migration chip for chemotaxis-based microfluidic selection of heterogeneous cell populations. *Sci. Rep.* **5**, 9980 (2015).

123. Virumbrales-Muñoz, M. *et al.* Enabling cell recovery from 3D cell culture microfluidic devices for tumour microenvironment biomarker profiling. *Sci. Rep.* **9**, 6199 (2019).

124. Donkor, J., Sariahmetoglu, M., Dewald, J., Brindley, D. N. & Reue, K. Three mammalian lipins act as phosphatidate phosphatases with distinct tissue expression patterns. *J. Biol. Chem.* **282**, 3450–7 (2007).

7. Supplementary information

Supplementary Table 7.1 Plasmids used in NIH 3T3 and U2OS transfections. Plasmids #1 were used to transfect NIH 3T3 cells, while plasmids #2 were used in U2OS cells.

Construct	Backbone	Source
Ctdnep1-GFP #1	pcDNA3.1(+)-C-eGFP (GenScript)	From the lab
Ctdnep1-GFP #2	pDONR201 (Life Technologies)	From the lab
Ctdnep1_D67E-GFP #1	pcDNA3.1(+)-C-eGFP (GenScript)	From the lab
Ctdnep1_D67E-GFP #2	pDONR201 (Life Technologies)	From the lab
Eps8L2-GFP	pcDNA3.1(+)-C-eGFP (GenScript)	From the lab
Myc-Eps8L2	pRK5mycGW (Fanny Jaulin Lab)	From the lab
Nep1-r1-HA-ProtA	pcDNA3.1 (Invitrogen)	Han, S. *et al.* 2012[76]
Lipin-2-V5-His	pcDNA3.1/V5-His (Invitrogen)	Donkor, J. *et al.* 2007[124]

Supplementary Table 7.2 Oligonucleotides sequences used to create the gRNAs for the CRISPR/Cas9 assays. FW: forward; RW: reverse.

Gene	Oligonucleotide sequence 5'-3'
CTDNEP1	FW CACCGGCTGTCACCAGAGCCTATGT
	RW AAACACATAGGCTCTGGTGACAGCC
EPS8L2 #1	FW CACCGTCCCTGACACTGGCTACCAC
	RW AAACGTGGTAGCCAGTGTCAGGGAC
EPS8L2 #2	FW CACCGGCGGTAGGACAACACTTACT
	RW AAACAGTAAGTGTTGTCCTACCGCC

Supplementary Table 7.3 Primers used in Ctdnep1 or Eps8L2 mutations screening in CRISPR/Cas9 assays. Guanine-Cytosine content (GC %), Temperatures of Melting (Tm) or of Annealing (Ta) and amplicon length were determined using SnapGene 2.8.2 software. FW: forward; RW: reverse.

Gene	Primer sequence 5'-3'	GC %	Tm (ºC)	Ta (ºC)	Amplicon length (bp)
CTDNEP1	FW CACAGCCCTTCTCAACCTTC	55	56	55	1022
	RW TTACAGGTATGGGGGATTGG	50	54		
EPS8L2	FW GGTCTCTTTGCTGGATTTGG	50	54	55	1006
	RW CAGTCCATTGGAGCAGATACC	52	56		

Supplementary Table 7.4 Antibodies used for immunofluorescence (IF) or Western blot (WB) analyses.

Antibody/Dye	Source	Reference	Working dilution
Chicken anti-GFP	Aves Lab	GFP-1020	IF 1:1000
Mouse anti-pericentrin	BD Biosciences	611814	IF 1:200
Rabbit anti-β-catenin	Invitrogen	712700	IF 1:200
Mouse anti-c-Myc	Invitrogen	13-2500	WB 1:500
Mouse anti-V5	Invitrogen	R960-25	WB 1:500
Goat anti-Chicken IgY (H+L) Secondary Antibody, Alexa Fluor 488	Invitrogen	A-11039	IF 1:800
Goat anti-Rabbit IgG (H+L) Highly Cross-Adsorbed Secondary Antibody, Alexa Fluor 555	Invitrogen	A-21429	IF 1:800
Goat anti-Mouse IgG (H+L) Highly Cross-Adsorbed Secondary Antibody, Alexa Fluor 647	Invitrogen	A-21236	IF 1:800
Goat Anti-Mouse IgG (H+L) - HRP Conjugate	Bio-Rad	1706516	WB 1:5000
Alexa Fluor™ 647 Phalloidin	Invitrogen	A22287	IF 1:100
DAPI	Sigma-Aldrich	D9542	IF 1:10 000

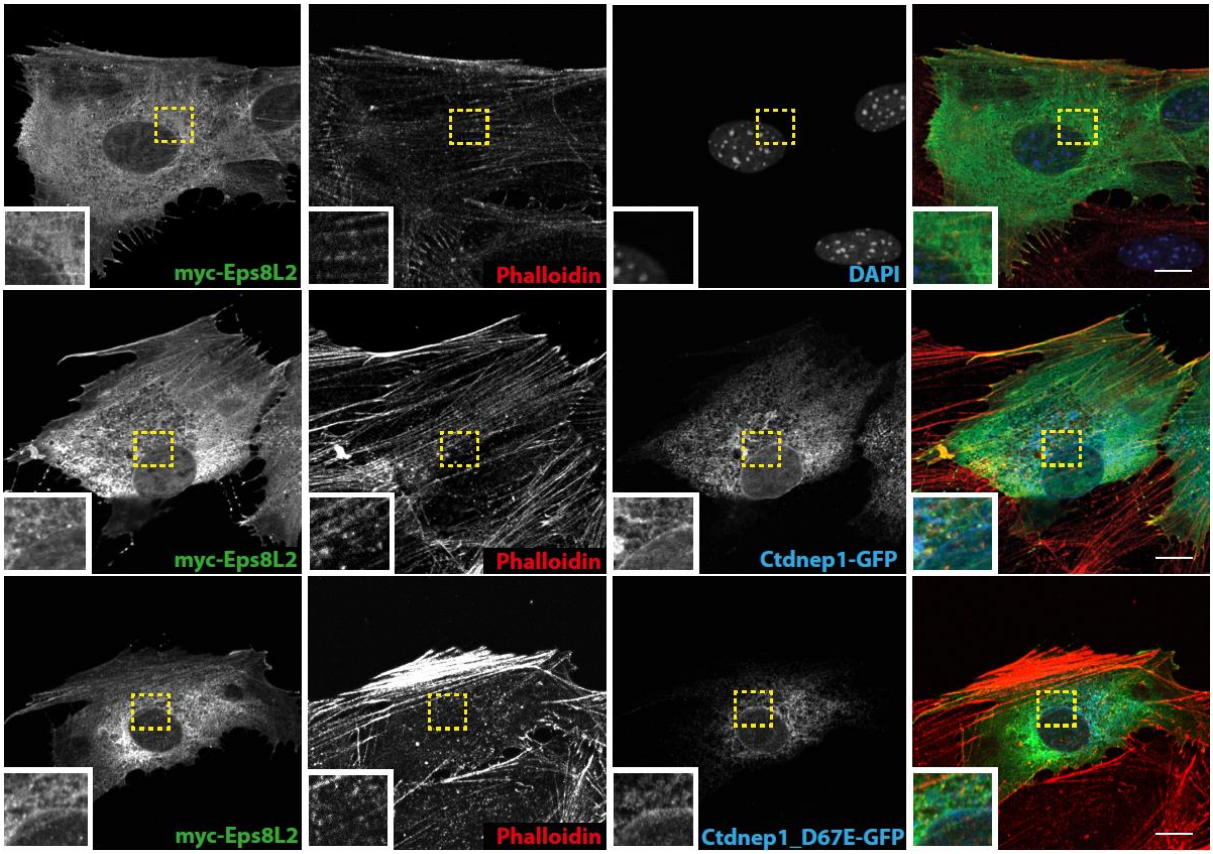

Supplementary Figure 7.1 Wound-edge fibroblasts stimulated with LPA and microinjected with Myc-Eps8L2, Ctdnep1-GFP and Ctdnep1_D67E-GFP. Cells were stained for Myc (Eps8L2) in green, phalloidin (F-actin) in red, DAPI (DNA) in blue and GFP (Ctdnep1 and Ctdnep1_D67E) in blue. The last image of each row results from the merging of all channels. The insets show enlarged views of the yellow regions. Scale bar: 10 μm. Adapted from Calero-Cuenca, F.J. *et al.* 2019[87].

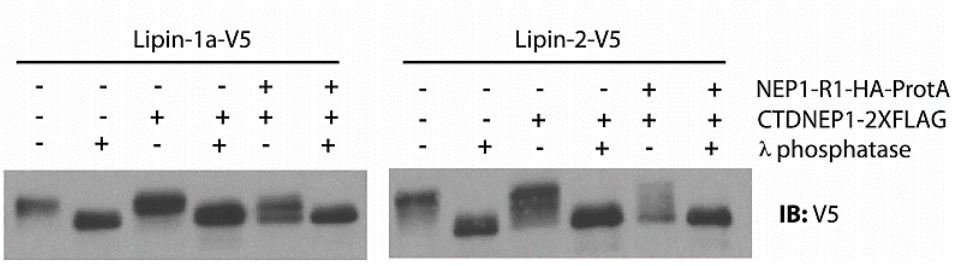

Supplementary Figure 7.2 Western blot analysis of total HEK 293 cells lysate expressing Lipin-1a-V5 or Lipin-2-V5 and Ctdnep1-2XFLAG alone or in combination with Nep1-r1-HA-ProtA. Lambda phosphatase treatment was performed to show that bands with lower molecular weight were due to dephosphorylation. This shows that Ctdnep1 can only dephosphorylate Lipin-1 or -2 in the presence of Nep1-r1. Adapted from Han, S. *et al.* 2012 [76].